1980

An inductively coupled plasma as an ion source for the determination of trace elements in solutions by mass spectrometry

Robert Samuel Houk
Iowa State University

HOUK, ROBERT SAMUEL

AN INDUCTIVELY COUPLED PLASMA AS AN ION SOURCE FOR THE DETERMINATION OF TRACE ELEMENTS IN SOLUTIONS BY MASS SPECTROMETRY

Iowa State University PH.D. 1980

An inductively coupled plasma as an ion source for the determination of trace elements in solutions by mass spectrometry

by

Robert Samuel Houk

A Dissertation Submitted to the
Graduate Faculty in Partial Fulfillment of the
Requirements for the Degree of
DOCTOR OF PHILOSOPHY

Department: Chemistry
Major: Analytical Chemistry

Approved:

Signature was redacted for privacy.

Signature was redacted for privacy.

In Charge of Major Work

Signature was redacted for privacy.

For the Major Department

Signature was redacted for privacy.

For the Graduate College

Iowa State University
Ames, Iowa

1980

TABLE OF CONTENTS

CHAPTER I. INTRODUCTION

One of the most pressing problems faced by modern analytical chemistry is the development of techniques for the determination of trace substances in the environment. As man continues to disturb natural levels of trace substances, reliable methodology useful for the identification and quantitative determination of trace levels of potentially dangerous substances in real samples becomes necessary. Trace elements are among the most important and potentially dangerous substances that man releases into his environment. The overall picture of the effects of abnormal levels of trace elements in humans, and in the environment in general, is one of extreme complexity, with interactive effects, various chemical states, and speciation effects likely to play major roles (1-6). Basic to an increased understanding and intelligent control of these effects are reliable analytical techniques for multielement determinations at trace levels. Certainly the most challenging problems relate to the study of interactive and speciation effects, which require analytical techniques capable of providing chemical information for trace elements, i.e., oxidation and coordination state and identity of ligands. New techniques for these problems will undoubtedly build upon reliable methods for the total amounts of those elements of interest, as most current methods for

trace elements provide little or no speciation information.

Solutions are among the most important samples for which trace elemental analytical techniques are required. Trace elements in body fluids provide useful diagnostic information for certain diseases. Large numbers of solid samples such as river sludge, biological tissue, soils, and minerals are conveniently digested and then handled as solutions. Solutions are important modes of intake of trace elements by most life forms. Humans directly ingest drinking water, inferring a need for accurate monitoring of trace elemental levels in water sources. Many marine forms eaten by humans are capable of concentrating trace elements from ambient water, e.g., arsenic in oysters and mercury in fish. These valuable food sources provide a potential hazard to humans from a sudden ingestion of large amounts of trace elements (5-6). These are among the reasons for the establishment of allowable levels of trace elements in water and other environmental sources. Curiously, many of the allowable levels set by the U. S. Environmental Protection Agency are not directly based on proven physiological effects but on the powers of detection of accepted analytical methods or the lack of definite information concerning the efficiency of treatment procedures for trace elements (7, 8).

Atomic absorption spectrometry (AAS) has found the widest scope of application among the accepted analytical

methods for trace elements in solutions. Although AAS has excellent figures of merit for single element determinations, and broad elemental coverage can be obtained through a variety of special techniques such as hydride generation, the method is unsuitable for the rapid determination of more than a few elements. This limitation is largely due to the lack of a tunable narrow line source of sufficient intensity and wavelength range. Atomic absorption spectrometry is also plagued by an inherently small dynamic range, necessitating sample dilution or alternate line selection for the application of proposed multielement AAS schemes to the analysis of solutions with a wide range of trace elemental concentrations. Techniques for multielement AAS will probably be impractical for more than 6 elements at one time (9, 10).

Thus, a major objective for the development of other methods of analysis of solutions for trace elements is that the new method be capable of multielement analysis in a practical sense. The capability to determine large numbers of elements will become increasingly attractive as monitoring programs become more comprehensive and as interactive effects between trace elements become better understood. Two general types of elemental determinations are suggested: a) survey analysis providing qualitative and semiquantitative information for nearly all the elements, and b) accurate quantitative analysis of selected elements in a simultaneous or rapid

sequential fashion. The developing method with both of these capabilities in a single instrument will fulfill two analytical needs that usually require separate instruments.

Other objectives for developing methods of trace elemental analysis of solutions include the following. The powers of detection should be sufficient to determine levels of interest of large numbers (>12) of trace elements under a single set of operating conditions. The method should be directly applicable to solutions with minimal pretreatment, because extensive sample handling procedures lengthen the analysis time, complicate the practical problems involved in continuous or on-line monitoring applications, and increase the likelihood of contamination. This criterion also infers the absence or limited presence of interference effects. The method should also possess sufficient dynamic range to determine the wide ranges of trace elemental concentrations in solutions without excessive dilution or preconcentration procedures. The method should be capable of rapid sample throughput with acceptable accuracy and precision as defined by potential analytical problems. Water monitoring problems essentially involve the determination of trace element levels as being above or below a defined value, whereas diagnostic or physiological applications may require accurate values for the levels of each trace element of interest. Isotopic abundance information for pertinent elements is a useful ca-

pability generally lacking in methods based on optical spectrometry. Physiological studies based on stable tracer isotopes of trace elements would be one application requiring isotopic determination. Geochemical age determinations and isotopic survey analysis of ores and minerals are other potential applications of a multielement method capable of providing isotopic information on solutions.

A variety of multielement methods for trace analysis are currently available. These methods may be broadly classified according to their instrumental principles as follows: a) nuclear, b) electrochemical, c) mass spectrometric, and d) optical spectrometric methods. A brief survey of the performance of these methods relative to the specified objectives is appropriate.

The major nuclear methods applied to trace analysis of solutions are X-ray fluorescence (XRF), proton-induced X-ray emission (PIXE), and neutron activation analysis (NAA). Conventional XRF generally lacks the powers of detection necessary for levels of interest of trace and ultratrace elements (<1 ug/mL) unless time-consuming sample preconcentration procedures are used (11). Both PIXE and NAA have excellent powers of detection and elemental coverage and are capable of isotopic determinations. Both techniques are capable of identifying trace elements without standards; PIXE can also provide useful quantitative multielement results for thin

solid samples without standards, e.g., air particulates deposited on filters (12). Quantitative PIXE determinations of thick samples are most efficiently performed with an internal standard (13), and quantitative NAA generally requires either an internal or closely-matched external standard irradiated under identical conditions as the sample (14). The accuracy and precision achievable by NAA is of the order of a few percent and is often superior to that obtainable by other trace multielement techniques, particularly near the limit of detection (14, 15).

For the multielement analysis of solutions, both PIXE and NAA often require significant sample treatment before or after irradiation, i.e., solution deposition and solvent evaporation or radiochemical separations in NAA. The corresponding delay in analysis time is further aggravated in NAA by the practice of long irradiation of a discrete sample followed by a time delay sufficient for the decay of potentially interfering short-lived nuclides. An inherently low sample throughput rate results for NAA despite automation of the sample transfer and data acquisition processes. A similar delay due to sample positioning in the excitation beam also limits the sample throughput rate of most PIXE facilities. A more fundamental limitation of PIXE is its lack of powers of detection for light elements ($Z<15$) due to low X-ray emission cross sections (12). Both techniques generally require com-

plex, expensive irradiation facilities unavailable to most laboratories.

Most of the applications of PIXE and NAA have concentrated on the determination of trace elements in small, discrete samples. A flow-through system for the direct determination of major and minor elements in fluids by NAA has been described (16); as yet, such systems have found little application for trace element determinations in solutions. A particular instrument employing PIXE for the direct multielement analysis of liquids has been described. For such an unfavorably thick sample as a hanging water drop, the detection limits obtained for the first row transition elements were approximately 1 ug/mL. Incredibly, this author used As for his internal standard (17)! In these most favorable cases for PIXE cross sections, the powers of detection are barely adequate for even the identification of levels of interest of trace elements in solution. Thus, the usefulness of PIXE for the direct multielement analysis of solutions at high sample throughput rates is presently marginal. Despite the proven analytical figures of merit of both PIXE and NAA, the development of multielement methods better suited for the analysis of solutions and more accessible to the general analytical community is justified.

Anodic stripping voltammetry (ASV) is the major electrochemical method to be applied to trace elemental anal-

ysis of solutions. This technique possesses excellent powers of detection for some of the most important elements, e.g., Cd and Pb, and can provide some speciation information for trace elements in favorable cases. Experimental problems with ASV include marginal resolution of stripping peaks from different elements, formation of stable intermetallic compounds during the stripping phase, potential interferences from electroactive organic compounds, and the need for an extremely close match between sample and standard matrix to insure reliable electrode response. In order to minimize these potential problems, most published procedures applying ASV to trace element determinations employ extensive preseparations and chemical preparation designed to optimize the specific determination of 1-4 elements (18). Because of the general necessity of such specialized procedures, ASV is of limited applicability for the rapid determination of more than a few elements in real samples under a single set of operating conditions. The present state-of-the-art of nuclear and electrochemical techniques for trace multielement analysis of solutions is impressive but not wholly satisfactory, particularly for the survey and quantitative determination of large numbers of elements at high sample throughput rates in solutions of widely varying composition.

The inherent capabilities of mass spectrometry make it one of the fastest growing techniques used in chemical analy-

sis. In many applications mass spectrometry provides qualitative and quantitative information, including isotopic abundances, with unsurpassed powers of detection. The successful interfacing of gas chromatographs with mass spectrometers has led to GC-MS hybrid instruments that have rapidly become the preferred approach for the analysis of mixtures of organic compounds extracted from many sources. Research programs in the various physical, medical, and environmental sciences are increasingly exploiting such information.

Despite the demonstrated utility of mass spectrometry for a variety of problems involving gaseous or solid samples, it is scarcely used for the routine determination of trace elements in solutions. Certainly no commonly used mass spectrometric method is likely to become widely accepted for the analysis of solutions, because present ion sources are not generally useful for the direct examination of liquid samples. Those methods that have been applied to solutions, such as spark source mass spectrometry, generally require extensive preliminary sample preparation procedures, e.g., the evaporation of solutions to dryness followed by formation of a conducting briquet from the solid residue. The pretreated sample is then physically introduced into the vacuum system; the associated time requirement for these operations renders the routine analysis of large numbers of liquid samples impractical.

In contrast, trace elements in large numbers of solution samples are commonly determined by atomic emission spectrometry. In this technique, solution aerosols are injected directly into a variety of vaporization-atomization-excitation-ionization (VAEI) cells. Such cells as arc or spark plasmas provide significant populations of positive ions detectable by mass spectrometric techniques. In fact, mass spectrometry provides invaluable diagnostic information for a variety of flames and plasmas similar to those used for trace elemental analysis. Because these VAEI cells operate at temperatures and pressures (≥2000 K, 1-1000 torr) that are intolerable for the operation of mass spectrometers (<300 C, $<10^{-5}$ torr), an appropriate interface is interposed. An approach based on the extraction of the ions from these cells, along with other gaseous constituents, through an orifice into a high vacuum system housing the mass spectrometer has been utilized to reduce the temperature and pressure of the extracted gas. The orifice thus acts as an interface between the high pressure, high gas temperature ionization cell and the much lower temperature and high vacuum conditions required by the mass spectrometer. This technique is presently used by several investigators for the fundamental study of various gas phase atomic or molecular processes (19-53). In these studies, emphasis has been placed on the observation of ions derived from the major cell

gases, e.g., inert gas monatomic and cluster ions in a variety of discharges. Ions derived from elemental constituents of analyte solutions introduced into an appropriate ionization cell should also be extractable by a similar approach. It should therefore be possible to combine the convenience and efficiency of introducing solution samples into an appropriate plasma with the analytical capabilities of mass spectrometry provided a suitable source-interface configuration can be developed.

Several types of plasmas have been coupled with mass spectrometry and applied to chemical analysis. The efficiency of ionization reactions at atmospheric pressure has been amply demonstrated by the development of atmospheric pressure ionization (API) for organic compounds. This ionization technique employed a weak plasma generated by a corona discharge or B-particle emitter. It possessed high powers of detection (approximately fg) for certain classes of organic compounds (54-62). In another analytical application, a hollow cathode discharge served as an ion source for mass spectrometry of solid samples (63-67). Gray has evaluated a system for trace element determinations based on the introduction of solution aerosols into a DC capillary arc plasma (CAP) (68). An interface similar to that used in the present work was employed. Background mass spectra obtained for the CAP were simple and had few peaks above 50 u. A variety of

trace elements in solutions were easily detected in a scanning mode at <1 ug/mL levels. Excellent powers of detection were obtained for the elements studied (69-73). The relative abundances of the various isotopes of Sr and Pb were determined with a relative precision of 0.5% in dissolved mineral samples (71, 72). Thus, the results obtained with the CAP indicated the feasibility of determining trace elements in solution by injecting an aerosol into a plasma for vaporization, atomization, and ionization, followed by ion extraction through an orifice into a high vacuum system housing a mass spectrometer.

Although both the CAP and the inductively coupled plasma (ICP) were originally developed for trace element determinations by atomic emission spectrometry, the ICP has found much wider application (74, 75). Most of the characteristics of the ICP that have vaulted it to supremacy as a VAEI cell for atomic emission spectrometry are also highly desirable in an ion source for mass spectrometry. Although definitive data for a direct comparison between the ICP and CAP are unavailable, the excellent performance of the ICP in atomic emission spectrometry leads to the expectation that the ICP will be eventually superior to the CAP as an ion source.

The desirable features of the ICP as a source of positive ions are described below:

1) At temperatures of 4000-8000 K, the relatively long resi-

dence time (2-3 ms) of analyte species and efficient injection of sample into the axial channel of the ICP assures effective vaporization, atomization, and ionization of the introduced sample (76-78). Although definitive data are lacking, the gas temperatures, residence time, and injection efficiency experienced by analyte species in the ICP are intuitively expected to be greater than those for the CAP

2) A high number density of trace element ions is inferred by the common use of emission lines from excited ions for the determination of trace elements by atomic emission spectrometry. For example, cadmium, despite its relatively high ionization potential (8.99 eV), is often determined using an ion line. The alkali metals are almost totally ionized in the plasma at observation heights approximately 10 mm from the load coil. Indeed, convincing evidence supports the occurrence of suprathermal ionization processes in the ICP. Such processes result in ion number densities in excess of the values predicted from local thermodynamic equilibrium (LTE) considerations (79-85).
3) The trace element ions are confined in the axial channel region of the ICP. This localization is important for efficient extraction of the ions into a mass spectrometer.
4) Two of the most troublesome interference effects commonly

observed in analytical atomic spectrometry are relatively unimportant in the ICP. The first effect is solute vaporization interferences caused by formation of refractory compounds during the vaporization of the solution aerosol. For example, the presence of a phosphate matrix suppresses the free atom formation, and hence the emission of atomic Ca species because refractory $Ca_2P_2O_7$ or $Ca_3(PO_4)_2$ is formed in the aerosol droplets during the vaporization process. The thermal stability of such compounds reduces the efficiency of free atom formation in most sources. In the ICP, however, the high temperature, efficient sample injection, and long residence time of analyte species result in efficient dissociation and free atom formation for trace elements in a wide variety of solution matrices (76, 86). The second effect is ionization interferences produced by easily ionizable elements. Gas phase ionization equilibria can shift unpredictably if the electron number density in the VAEI cell changes from sample to sample. Changes in the concentrations of easily ionizable elements such as the alkali metals commonly cause such fluctuations in flames and in many electrically-generated plasmas. However, in the ICP the electron number density changes only slightly for Na concentrations from 0 - 700 ug/mL. Various suprathermal ionization processes have also been invoked to explain the

apparent presence of an "ionization buffer", namely, the supporting Ar atmosphere (80, 84, 85). Whatever the cause, matrix effects caused by ionization interferences are much less significant in the ICP than in flames and other plasmas (86, 87).

The VAEI processes in the ICP are remarkably independent of the solution matrix. This independence undoubtedly contributes to the extensive linear dynamic range (4-5 orders of magnitude) observed in analytical calibration curves obtained by atomic emission spectrometry (76, 77, 88).

Analyte ions extracted from an ICP should yield a simple mass spectrum relatively free from mass spectral interferences, enabling the use of a medium resolution quadrupole mass analyzer. The following reasons support this expectation. The chemically inert argon atmosphere and high gas temperature should limit the formation of molecular ions containing trace elements. Extensive formation of multiply charged ions is also unlikely. Most second ionization energies are above 14 eV. Ionization processes in the ICP operated at atmospheric pressure are essentially thermal or collisional and are expected not to be energetic enough for extensive formation of multiply charged ions. Ion optical conditions should be nearly ideal for a quadrupole mass spectrometer. The ions present in the ICP should be at nearly thermal energies because of the very short mean free path and

low ratio of electric field to pressure. The ICP should have a fairly simple and uncluttered background mass spectrum. Argon ions, argon cluster ions, atmospheric ions, and water fragment and cluster ions are expected from the ICP, as such ions are commonly observed from other plasmas or flames (27, 31-38, 48, 49, 54-66). The m/z values at which these potentially interfering ions occur, e.g., H_3O^+ and Ar^+, are predictable and yield prohibitive interference with only a few trace elements of interest.

The objective of the present work is to present preliminary results and evaluate the potential utility of inductively coupled plasma-mass spectrometry (ICP-MS) for the determination of trace elements in solutions. The next section discusses the basic principles of the development of this technique.

CHAPTER II. APPARATUS AND PROCEDURES

A schematic diagram illustrating the ICP-MS technique is shown in Figure 1. The physical processes upon which this approach is based may be summarized as follows:

1) The sample solution is nebulized, taken up by an argon stream (called the aerosol gas flow), and desolvated. The resulting gas stream contains small solid particles whose composition is characteristic of the sample solution.
2) The aerosol gas flow is injected into the ICP, which efficiently vaporizes the small solid particles. The high gas temperature promotes efficient atomization and ionization, resulting in a significant number density of ions derived from the trace elements in the sample. These analyte ions are localized in the axial channel region of the ICP.
3) The ICP next encounters the first part of the interface, i.e., a water cooled, conical skimmer centered on the torch. The axial channel region streams through the skimmer, forming an atmospheric pressure plume rich in sample ions. The remnants of the eddy current (outer) region of the ICP are deflected outside the skimmer.
4) The partially-extracted plume impinges on a water-cooled copper cone (called the sampler). A small molybdenum disk (called the orifice disk) containing an orifice resembling

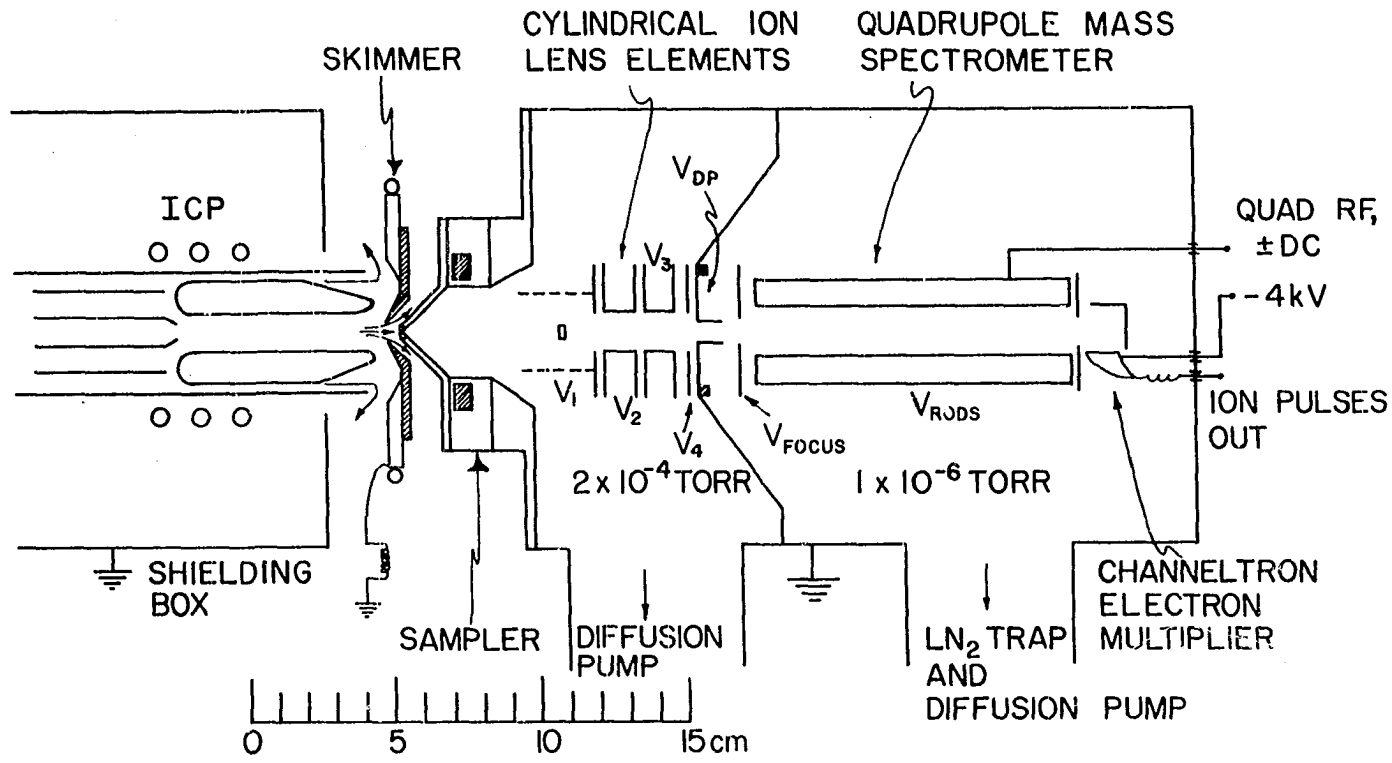

Figure 1. Schematic diagram of ICP, interface, and vacuum system.

a pinhole (50-70 um diameter) is sealed into the tip of the sampler. This assembly is mounted on the first stage of a differentially pumped vacuum system. A composite boundary layer forms between the flowing plume and the sampler because the sampler disturbs the plume in both an aerodynamic and electrostatic fashion. Most of the plume gas is deflected around the sampler. A small fraction of the plume gas with its ions is extracted through the boundary layer and orifice into the vacuum system.

5) As the gas particles are extracted into the vacuum system, their temperature and pressure are drastically reduced. A supersonically expanding jet of extracted gas forms inside the vacuum system. As the pressure in the jet decreases, the collision frequency decreases and the mean free path increases. Thus the composition of the extracted gas becomes constant at some point in the vacuum system.

6) The extracted particles consist of ions, electrons, and neutral species. After the supersonic expansion is essentially complete, the positive ions are collected and focused into a beam by an electrostatic ion lens system, while the unwanted neutral species and electrons are pumped away.

7) For orifice diameters ≥50 um and practical pumping speeds, the pressure in the first stage is too high for

operation of a quadrupole mass analyzer. Therefore, the ion lens transmits the ions through a circular aperture leading to a second, differentially pumped vacuum chamber. Because of the speed of the second pumping system and the limited conductance of the aperture between stages, the pressure in the second stage is low enough for operation of a quadrupole mass analyzer ($\leq 5 \times 10^{-5}$ torr).

8) The ions are directed from the differential pumping aperture through the field region of a quadrupole mass analyzer. For particular values of the DC and RF voltages applied to the quadrupole rods, only ions of a specific m/z value are transmitted along the quadrupole axis. Ions of other m/z values are deflected from the quadrupole axis and are lost.

9) The m/z resolved ions emerging from the mass analyzer strike the cathode of a Channeltron electron multiplier operated in a pulse counting mode. The resulting pulses are conducted from the multiplier anode to a counting preamplifier, discriminator, and counter. The m/z values at which counts are detected provide a qualitative identification of the trace elements in the original sample. The count rate at each m/z value is quantitatively related to the solution concentration of the corresponding trace element.

The following discussion concentrates successively on each of the above processes. The discussion also describes the equipment and procedures used in the present work and complements the summary presented in Table I.

Solution Nebulization

A variety of pneumatic or ultrasonic nebulizers are commonly used in analytical atomic spectrometry. The present work was performed with an ultrasonic nebulizer based on the design of Olson et al. (89). This nebulizer is shown in detail in Figure 2. The sample solution is transported by a peristaltic pump to the flat outside surface of a quartz cup. An ultrasonic transducer consisting of a piezoelectric crystal is mounted on the inside of the cup. Radiofrequency (RF) power applied to the transducer from an appropriate power supply induces crystal oscillations at ultrasonic frequencies. These oscillations are coupled through the quartz wall to the surface wetted by the sample solution, causing a fraction of the solution to be ejected from the surface as a mist of fine droplets. This mist is taken up by the aerosol gas flow and is transported through a desolvation apparatus. A heated chamber evaporates the solvent. An ice water cooled condenser removes most of the solvent (approximately 95%) (90). The resulting aerosol gas flow (approximately 1 L/min)

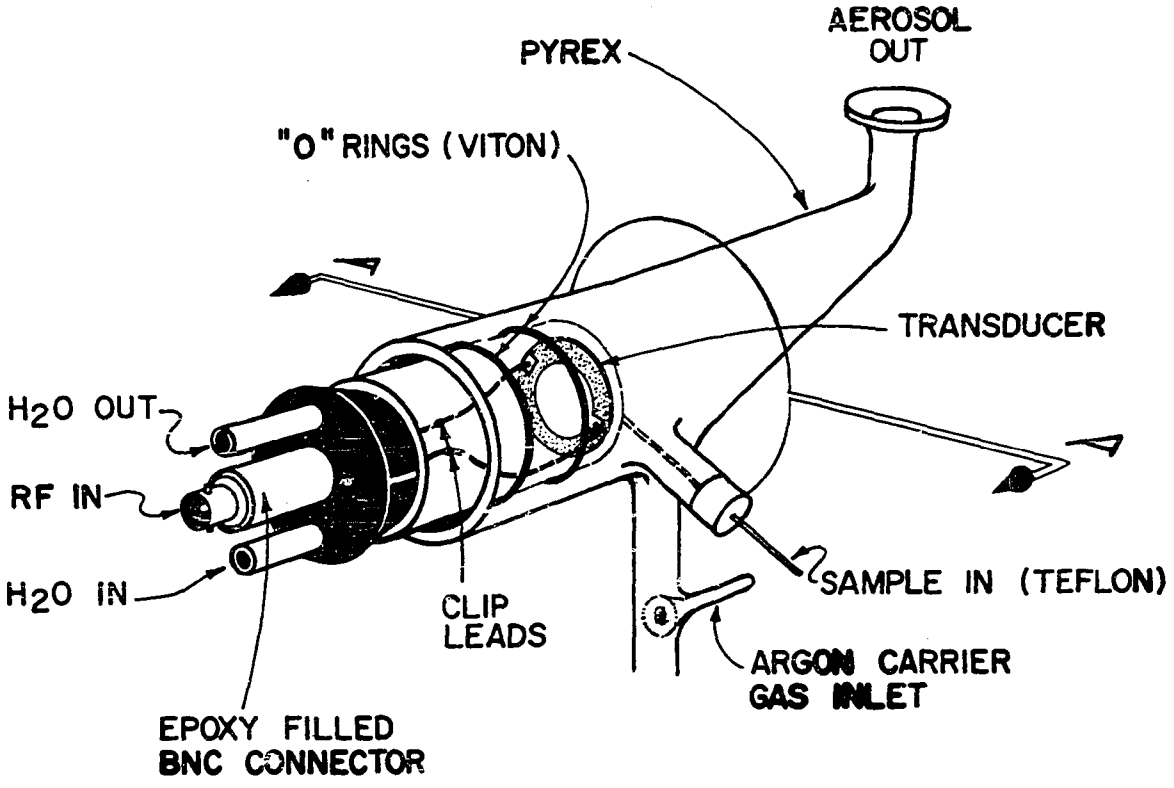

Figure 2. Ultrasonic nebulizer and spray chamber.

Table I. Instrumental Facilities.

Component Description Manufacturer	Operating conditions
Plasma generator: Type HFP-2500D with impedance matching network. Plasma-Therm, Inc. Kresson, NJ 08053	Forward power 1000 W. Reflected power <10 W. 27.12 MHz.
Plasma torch: All quartz Ames Laboratory design and construction with outer tube extended 50 mm above tip of aerosol tube (see Figure 4).	Argon flow rates: plasma flow 12 L/min. aerosol carrier flow 1 L/min. auxiliary flow used only during ignition.
Ultrasonic Nebulizer: Model UNS-1 Plasma-Therm, Inc. Kresson, NJ 08053 Similar to Ames Laboratory design. Modified Margoshes-Veillon desolvation system.	Sample introduction rate: 2.5 mL/min. by peristaltic pump. Transducer power 50 W. Transducer and condenser ice water cooled.
Orifice disk: Molybdenum disk. Agar Aids Stansted, Essex, England CM24 8DA	2 mm OD. 0.5 mm nominal thickness. Orifice length = orifice diam.
Vacuum system: Welded stainless steel assembly, differentially pumped Ames Laboratory construction	First stage pressure: 1 x 10^{-3} torr (air, 1 atm, 25°C). 4 x 10^{-4} torr (ICP sampling). Second stage pressure: 1 x 10^{-6} torr (ICP sampling).
Ion lens elements: Stainless steel. Based on Model 275-N2 Extranuclear Laboratories, Inc. Pittsburgh, Pa 15238	Voltage values: V_1 = -200V V_{DP} = -60 V_2 = -80 V_3 = -95 V_{FOCUS} = -18 V_4 = -60 V_{RODS} = -11

Table I. (continued)

Ion lens voltage supply Model 275-L25 Extranuclear Laboratories, Inc. Pittsburgh, PA 15238	Operated in atmospheric pressure ionization mode (electron impact ionizer off).
Quadrupole mass analyzer Model 100C. Uthe Technologies, Inc. (UTI) Sunnyvale, CA 94086	Minor modifications described in text.
Detector Channeltron electron multiplier Model 4717 Galileo Electro-Optics Corp. Sturbridge, MA 01518 Supplied by UTI.	Cathode bias -4kV. Gain = 10^6. Anode electrically isolated from channel.
Pulse counting system: Model 1121 preamplifier-discriminator. Model 1109 counter. EG&G Princeton Applied Research Princeton, NJ 08540	Single discriminator mode, threshold 3 mV.
Data acquisition (scanning mode): Active low pass filter-amplifier. Model 1020 Spectrum Scientific Corp. Newark, NJ 19711	Spectrum recorded on X-Y recorder: Y axis: filtered and amplified DC voltage (proportional to count rate from counter). X axis: DC voltage (0-+10v) from mass spectrometer controller (proportional to transmitted mass).
Data acquisition and handling (single ion mode): Counter interfaced to teletype for paper tape, hard copy record.	Mass spectrometer manually peaked on mass of interest, count period 10 s, 5 to 10 count periods recorded and averaged at each mass and for each solution.

contains fine solid particles (0.1-10 um diameter) characteristic of the sample solution. These conditions are convenient for introduction of solutions into an ICP.

This nebulizer is superior to other ultrasonic and pneumatic nebulizers in several respects. Olson et al. indicate a nebulization efficiency of approximately 10% for this ultrasonic nebulizer, compared to approximately 1% for state-of-the-art pneumatic nebulizers. The shielding of the ultrasonic transducer behind the quartz plate protects the transducer from chemical attack and permits efficient cooling, thus providing a useful lifetime of several months. Samples are easily changed with rapid cleanout (approximately 2 minutes) and negligible memory because of the continual introduction of solution. Detection limits for most elements obtained by inductively coupled plasma - atomic emission spectrometry (ICP-AES) are better by about one order of magnitude with this ultrasonic nebulizer compared to typical pneumatic nebulizers. Furthermore, the nebulization rate is independent of the aerosol gas flow rate, which allows the latter parameter to be optimized independent of the nebulization efficiency. Desolvation of the aerosol gas flow prevents "poisoning" of the ICP, which results when large amounts of molecular species, i.e., H_2O, are introduced (89). This nebulization-desolvation system represents the most efficient technique available for continous nebulization of so-

lutions, particularly when high powers of detection are desired.

ICP Formation and Aerosol Injection

The generation and stabilization of ICP's at atmospheric pressure was first demonstrated in 1942 by Babat (91). This research was performed during the seige of Leningrad and was forcibly interrupted when the German bombardment knocked out the electrical power generators supplying Babat's laboratory. Improved techniques for the stabilization and thermal isolation of ICP's were described in the early 1960's by Reed (92), who also recognized their capabilities as excitation sources for atomic spectra. Investigation of the usefulness of ICP's as VAEI cells for trace element determinations by AES were begun independently in 1962 at the Ames Laboratory, Iowa State University and at the laboratories of Albright and Wilson, Oldbury, England (74, 75). The powers of detection and analytical utility of ICP's were gradually improved by systematic optimization of operating parameters such as a) reduction of RF interference in the recording electronics, b) impedance matching between the RF generator and ICP, c) forward power regulation, d) aerosol generation, and e) aerosol injection efficiency through variation of plasma geometry (76). A number of ICP-AES facilities of two basic va-

rieties have been described, i.e., direct reading polychromators (77) or scanning monochromators (77, 93, 94).

The ICP used in the present work is generated and sustained in a plasma torch similar to the one shown in Figure 3. This torch represents the result of several years of experimental work involved in the adaptation of Reed's concepts of vortex stabilization of atmospheric pressure plasmas. The torch consists of an assembly of concentric quartz tubes, which serves to confine and define the argon flow patterns that sustain the ICP. The main argon flow (called the plasma support flow) is injected tangentially and spirals from the open torch end between the outer and auxiliary tubes. This vortex-like flow pattern is largely preserved as it passes the end of the auxiliary tube into the torch region enclosed by the load coil. Prior to ignition of the plasma a "seed" of electrons is provided with a Tesla coil. These electrons interact with time-varying magnetic fields induced by an RF current flowing in the load coil. The axially-oriented, induced fields cause the electrons to flow in closed annular paths inside the torch. Because this region is at atmospheric pressure, the mean free path is very short (approximately 10^{-4} cm) and the charged particles collide frequently with neutral species. The resulting resistance to their induced flow causes Joule or ohmic heating, which raises the temperature and causes further ion-

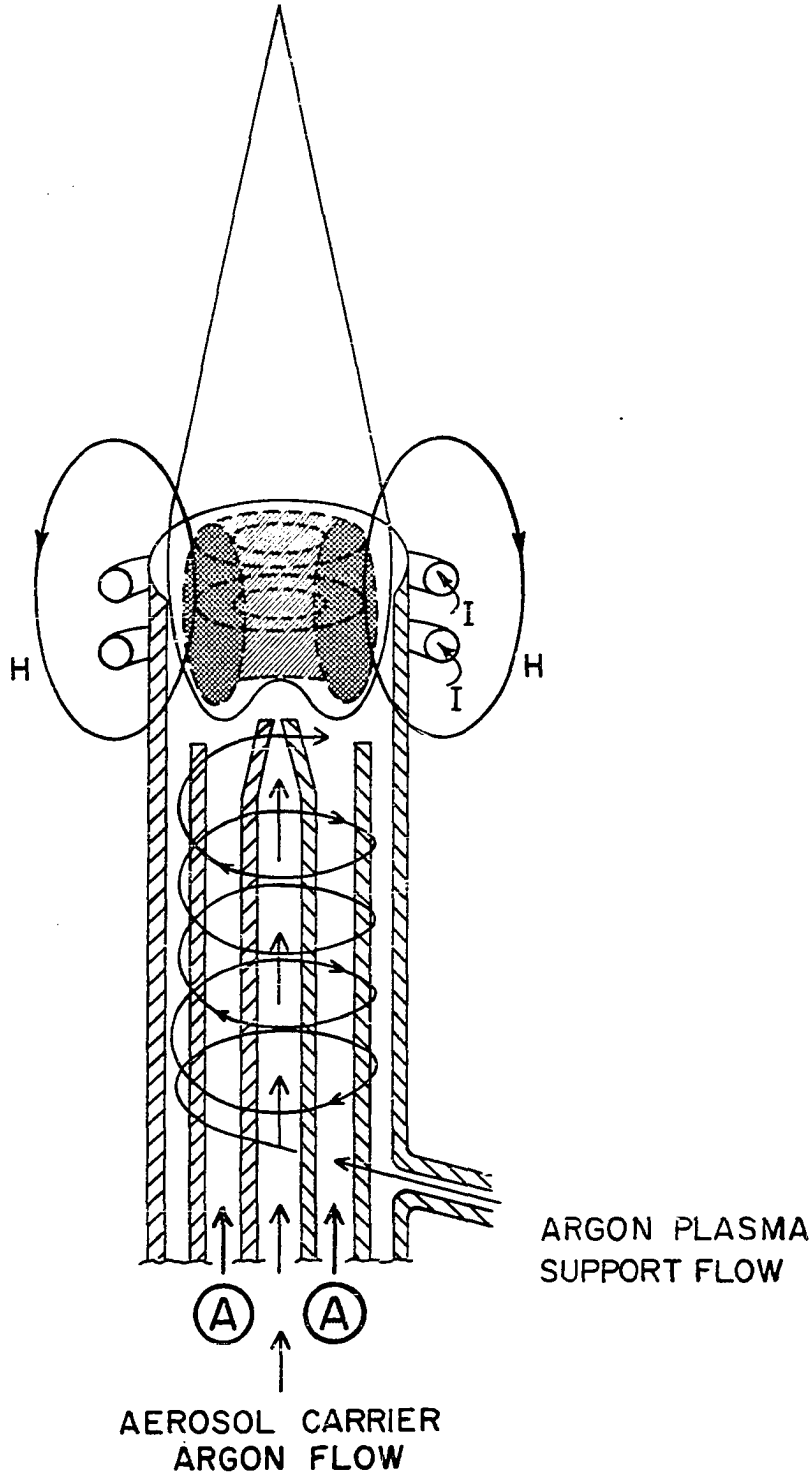

Figure 3. Schematic diagram of ICP torch, gas flows, and induced fields. Ⓐ denotes auxiliary gas flow.

ization. If the output impedance of the RF generator is carefully matched to that of the incipient plasma, RF power from the generator becomes efficiently coupled to the growing discharge. An extended plasma is thus formed in a few seconds. The gas flow containing the solution aerosol is then injected through the aerosol tube into the center of the plasma, causing the plasma to assume a toroidal configuration. The toroid consists of two clearly visible regions:

1) the outer region, called the toroidal or eddy current region. Because of the skin depth effect, nearly all of the RF power sustaining the plasma is coupled to this region (76, 94, 95). Maximum gas temperatures are obtained in the eddy current region (approximately 10,000 K, Figure 4) (78).
2) the inner region, called the axial channel. This region acts as the VAEI cell, as a large fraction of the solution aerosol is injected into it. Gas temperatures in the axial channel are somewhat lower than in the eddy current region. However, they are far higher than the gas temperatures in flames (78). Along with the high gas temperature, the long residence time (approximately 3 ms) of analyte species promotes efficient vaporization, atomization, and ionization of the aerosol particles. The atoms and ions remain dispersed in a high temperature argon atmosphere, whose chemical inertness (relative to

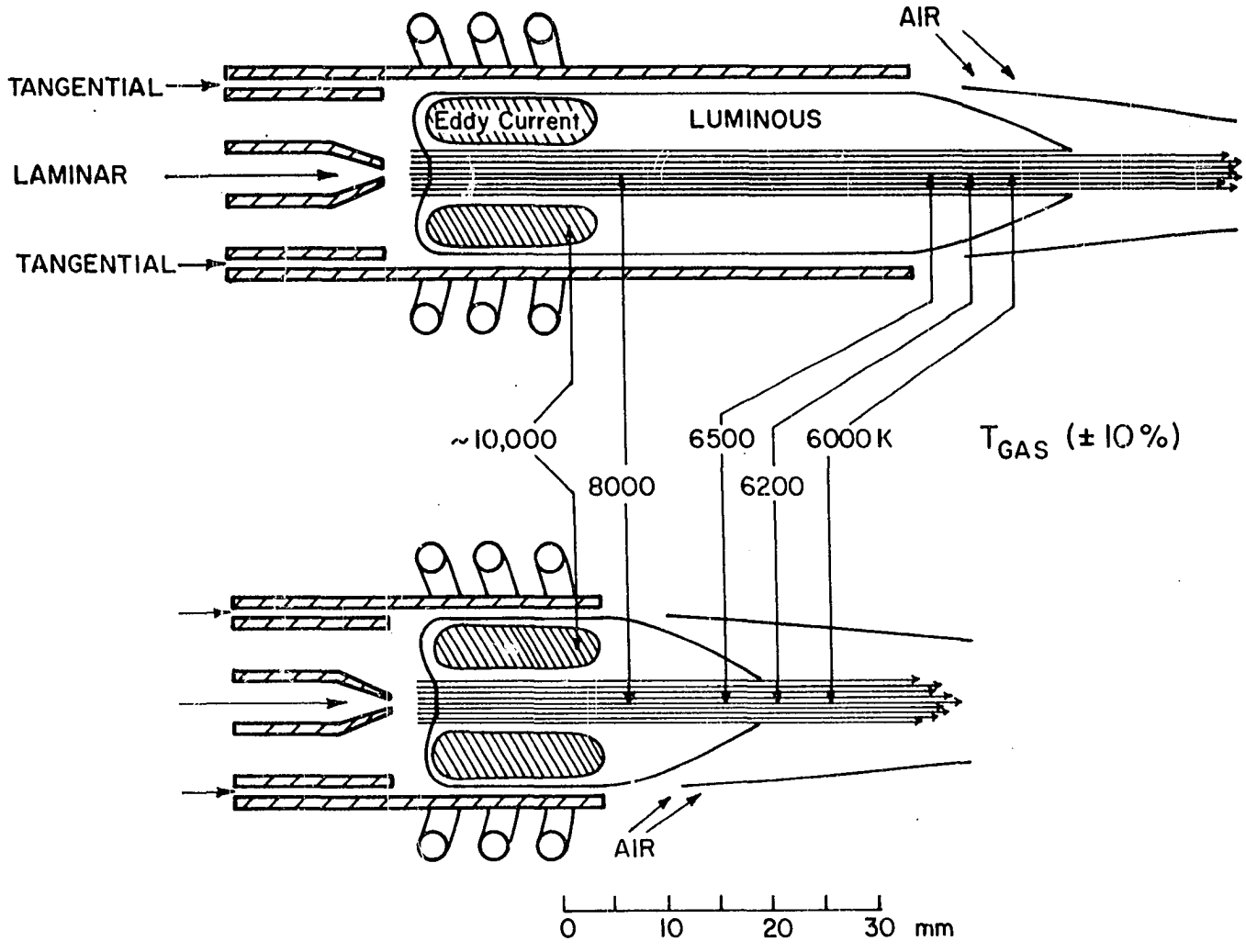

Figure 4. Estimated gas temperatures in ICP's generated in a) extended torch used in present study (top), and b) standard torch (bottom).

flames, for example) also inhibits formation of troublesome molecular species containing the analyte (76).

Both the plasma and aerosol gas flows also thermally isolate the plasma from the torch. This cooling prevents the torch from melting at the high gas temperatures of the plasma. The ICP is not contaminated by electrode material like arc-spark plasmas, because no electrodes are physically exposed to the discharge. Viewed from the open end of the torch the ICP looks like a luminous doughnut, with the brighter eddy current region enclosing the relatively darker axial channel. Viewed from the side the ICP looks like a wide flame consisting of an outer bright white section, i.e., the eddy current region, split by the relatively dark axial channel.

In the present study, the ICP was generated in a torch fitted with an extended outer tube as shown in Figure 1. The extension made it more convenient to accommodate various sampling devices during the development of the ion sampling interface. The outer tube merely elongated the ICP relative to its dimensions in torches of conventional length. The torch was operated horizontally. As viewed from its end, the extended ICP had its usual toroidal appearance displaying a relatively darker axial channel surrounded by a bright eddy current region. The torch was enclosed in a grounded, copper-lined shielding box, which greatly reduced noise

levels due to RF interference in the pulse counting equipment, ion gauges, and recorder associated in the vacuum system and mass spectrometer.

The estimated gas temperatures (T_{GAS}) in the ICP generated in the extended torch are compared with measured temperatures for the shorter, conventional torch in Figure 4 (78). The extension of the outer tube prevents air entrainment. Therefore, T_{GAS} for the extended torch remains higher than that in the shorter torch at the same distance from the load coil. For example, T_{GAS} in the axial channel opposite the end of the outer tube of the extended torch is estimated to be 6500 K. This T_{GAS} is equal to that at 15 mm from the load coil of the shorter torch. In other words, the cooling produced by argon confinement for 5 mm, followed by air entrainment for 10 mm (short torch) is taken tc be equal to the cooling produced by confining the argon for 25 mm in the extended torch.

Local Thermodynamic Equilibrium (LTE) Model of Analyte Ionization

The total number density of elemental species (designated $(n_M)_t$) in the axial channel of the ICP may be estimated from Equation (1),

$$(n_M)_t = \frac{R_{NEB} E_{NEB} E_{ICP} N_O T_{ROOM}}{F_{AER} T_{GAS} M} C_M \qquad (1)$$

where R_{NEB} = solution uptake rate of nebulizer (2.5 mL/min)

E_{NEB} = nebulization efficiency (10%) (89)

E_{ICP} = injection efficiency of aerosol into axial channel (visually estimated to be 75%)

F_{AER} = aerosol gas flow rate (1 L/min)

N_O = Avogadro's number

M = atomic weight of element M (g/mole)

T_{GAS}, T_{ROOM} = absolute temperature of axial channel and room, respectively

C_M = solution concentration of element M (ug/mL).

Substitution into Equation (1) with appropriate correction for units gives the following form.

$$(n_M)_t \ (cm^{-3}) = \frac{3.4 \times 10^{16}}{T_{GAS} M} C_M \ (\mu g/mL) \qquad (2)$$

The next objective is to calculate the fraction of $(n_M)_t$ that is ionized at ICP temperatures.

An indication of the efficiency of ionization processes in the ICP can be derived from a model based on the assumption that local thermodynamic equilibrium (LTE) exists throughout the ICP. The LTE concept is useful for many real plasmas, which are never in complete thermodynamic equilibrium because of photon emission and the presence of temperature

gradients. This difficulty is circumvented by the assumption that each small volume element has its own local temperature T. Within each volume element a common value of T defines the plasma properties and composition, i.e., all species have a Maxwellian velocity distribution and a Boltzmann distribution of the populations of bound energy states. The local temperature of each volume element is then considered to vary with position to account for the macroscopic temperature gradients present in the plasma (96-98), as indicated in Figure 4.

Regarding analyte ionization, the fundamental criterion for the validity of LTE is that ionization and ion - electron recombination are equilibrated, i.e., they occur at the same net rate regardless of the particular elementary reactions involved. The following equations apply to each volume element at its own local temperature (96).

$$M \leftrightharpoons M^+ + e \qquad \Delta E = IE_M \tag{3}$$

$$K = \frac{n_{M^+}\ n_e}{n_M} = \frac{(2\pi MkT/N_o)^{3/2}}{h^3}\left(\frac{2\ Q_{M^+}}{Q_M}\right)e^{-(IE_M)/kT} \tag{4}$$

$$\log K = \frac{3}{2}\log T - \frac{5040\ (IE_M)}{T} + \log\frac{Q_{M^+}}{Q_M} + 15.684 \tag{5}$$

In Equations (3) - (5) n_{M^+} , n_M , and n_e = number densities (cm^{-3}) of analyte ions, analyte atoms, and electrons, respec-

tively, IE_M = ionization energy (eV) of the element M, and Q_{M^+} and Q_M = electronic partition functions of the ion and atom, respectively, k and h = Boltzmann and Planck constants, respectively. The degree of ionization α is expressed in the following equations.

$$\alpha = \frac{n_{M^+}}{n_{M^+} + n_M} = \frac{n_{M^+}}{(n_M)_t} \tag{6}$$

$$1 - \alpha = \frac{n_M}{n_{M^+} + n_M} \tag{7}$$

$$K = \frac{\alpha\, n_e}{1 - \alpha} \tag{8}$$

$$\alpha = \frac{K}{n_e + K} \sim n_{M^+} \tag{9}$$

$$1 - \alpha = \frac{n_e}{n_e + K} \sim n_M \tag{10}$$

$$\log \frac{\alpha}{1 - \alpha} = - \log n_e + \frac{3}{2} \log T - \frac{5040\ (IE_M)}{T} + \log \frac{Q_{M^+}}{Q_M} + 15.684 \tag{11}$$

$$n_{M^+} = \alpha (n_M)_t$$

$$n_{M^+}(cm^{-3}) = \frac{3.4 \times 10^{16}}{MT}\ \alpha\ C_M\ (\mu g/mL) \tag{12}$$

In the present work, the partition functions Q_{M^+} and Q_M are calculated as functions of temperature by the polynomial expansion method of de Galan et al. (99), i.e.,

$$Q_{M^+} = a + bT + cT^2 + dT^3 + eT^4 + fT^5.$$

Although the values of the expansion coefficients a, b, c, ... were specified to be valid in the temperature range 1500-7000 K, they are used in the present work from 4000-10,000 K in lieu of another collection expressed as a convenient function of temperature. Certainly this procedure is more accurate than arbitrarily deleting the partition function terms from the above equations

The degrees of ionization (Equation (11)) expected under LTE for several elements of a range of ionization energies are shown as a function of T in Figure 5. At the highest axial channel temperature (approximately 8000 K, Figure 4), all the elements chosen are extensively ionized. From Figure 5 and Equation (12), for Cd at 50 ug/mL and 8000 K, $\alpha = 0.93$, and $n_{M^+} = 2 \times 10^{12}$ cm^{-3}. In each small volume element the ICP is electrically neutral in a macroscopic sense.

$$n_e = n_+ = n_{Ar^+} + \Sigma\, n_{H_xO^+} + \Sigma\, n_{M^+} \qquad (13)$$

Thus the electron number density equals the sum of the posi-

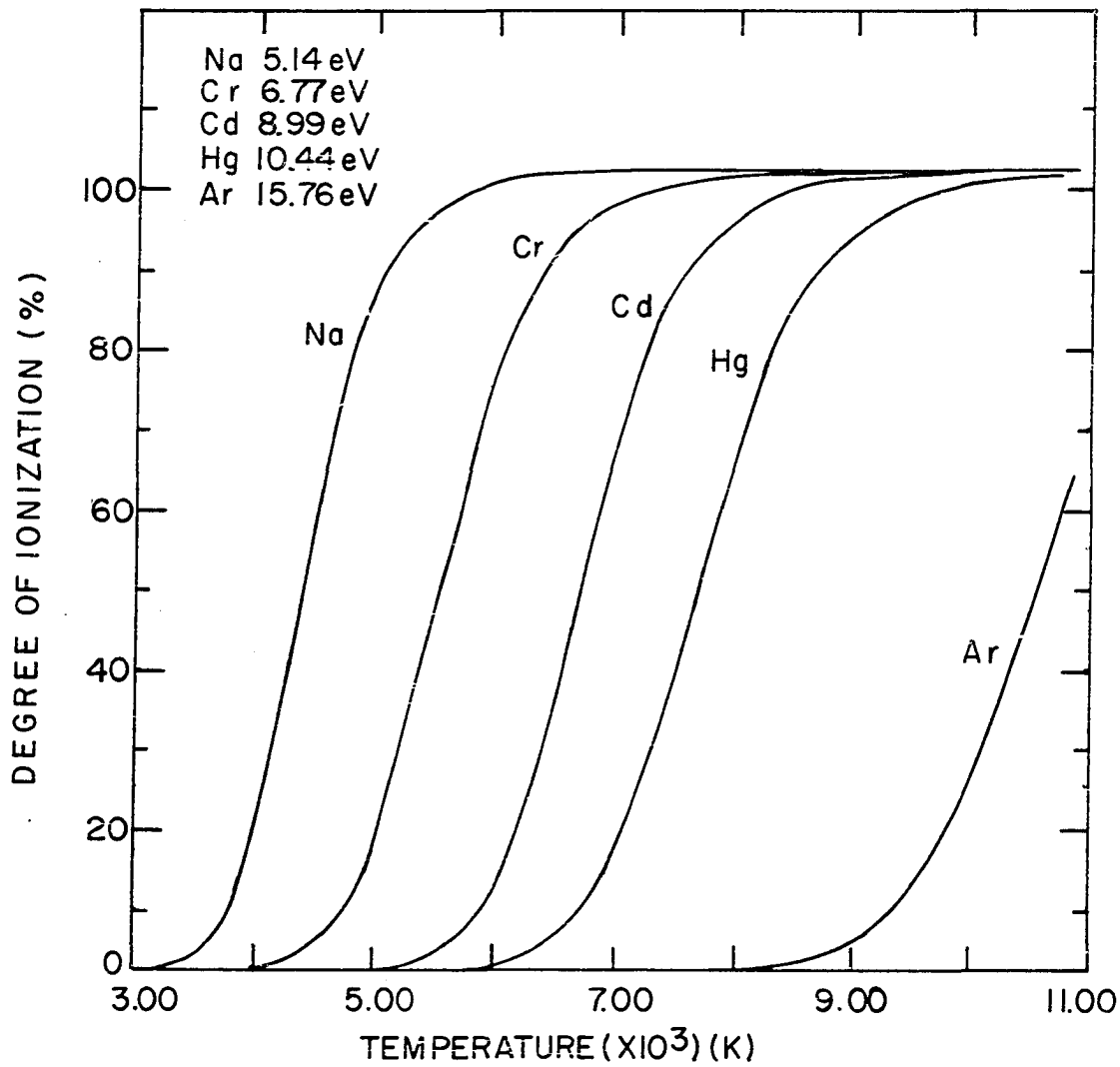

Figure 5. Degree of ionization calculated from Saha Equation for selected elements as a function of temperature, $n_e = 1 \times 10^{15}$ cm^{-3}.

tive ion number densities, i.e., the argon ions, ions derived from water (H_xO^+), and the analyte ions. Possible formation of negative ions is neglected in Equation (13). Because n_e = 10^{14}-10^{15} cm^{-3} in the ICP, the ions from trace levels of analytes, despite their extensive degree of ionization, make up a minor contribution to the total number of positive ions (79). This characteristic of the ICP helps explain its relative freedom from ionization interferences, as previously described (86, 87).

Ion Sampling Interface--Design Considerations

In the following discussion, several terms are used with specific connotations as shown in Figure 6. The term interface refers to the apparatus physically interposed between the ICP and vacuum system. The term orifice disk (#2 in Figure 6) refers to a small metal disk through which a cylindrical channel (#1) resembling a pinhole is drilled. The orifice disk is mounted in the tip of the water cooled sampler cone (#3), which in turn is attached to the vacuum system. The disk and cone tip together are referred to as the orifice assembly.

As the flowing plasma encounters the orifice disk and sampler cone, an aerodynamic disturbance results from the consequent deflection of the ICP gas. The disturbance is

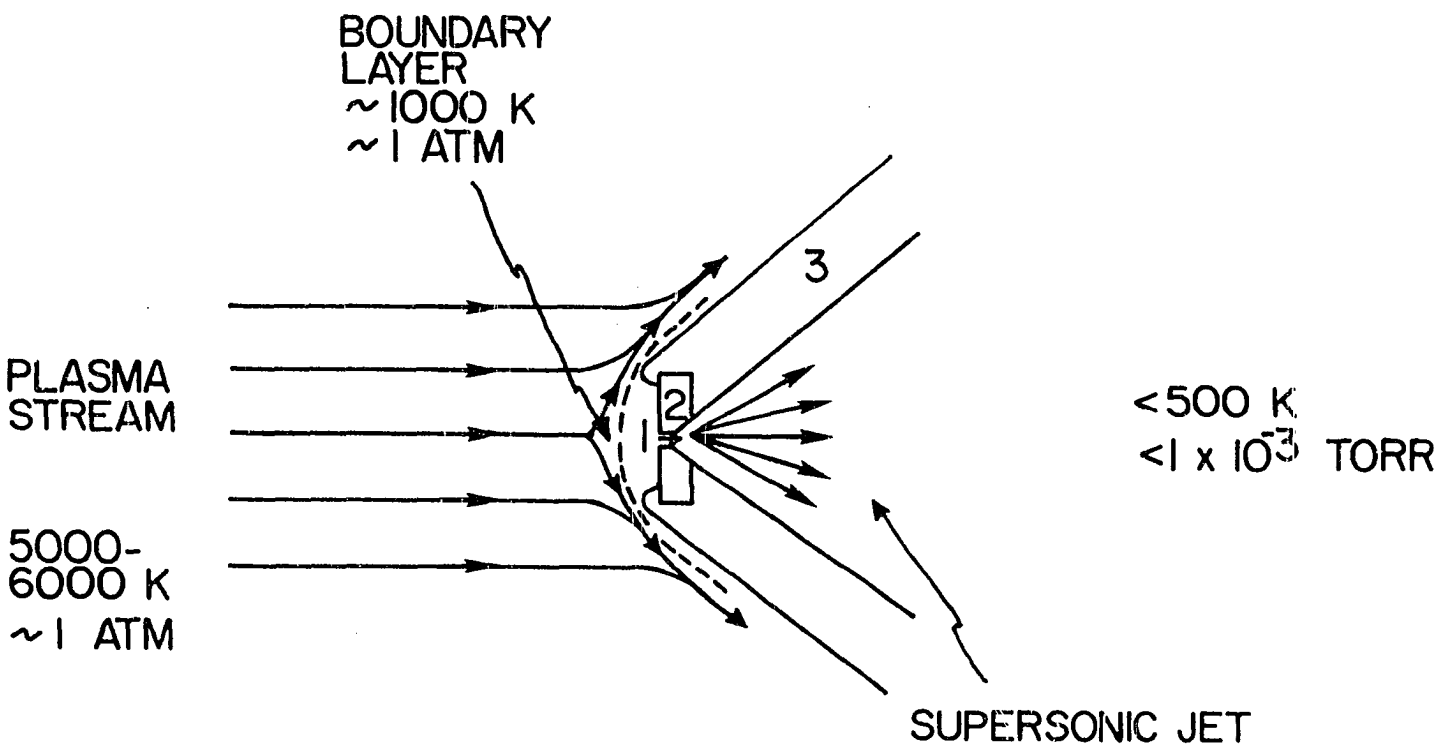

Figure 6. Physical processes occurring during sampling from atmospheric pressure source.

minimal for a finely pointed tip, because the gas is efficiently swept down the outside of the cone. However, if the cone tip is flat or recessed, an aerodynamically stagnant layer of gas forms between it and the flowing plasma (35, 44, 100, 101). This stagnant layer is in thermal contact with the relatively cool orifice assembly and is therefore much cooler than the flowing plasma stream. This layer thus presents an aerodynamic barrier to the extraction of ions from the ICP through the orifice.

On a microscopic scale, ions and electrons in the vicinity of the sampler are distributed spatially so as to oppose any difference in electrical potential between the ICP and the sampler. The difference in mobility between ions and electrons leads to a space charge accumulation adjacent to the sampler (19, 29, 102). The plasma sheath thus formed is illustrated schematically in Figure 7. This sheath is analogous to the electrical double layer formed between an electroactive surface and nearby bulk solution during voltammetric measurements. If this sheath extends across the orifice, ICP particles must be transported through the sheath before being extracted. The sheath thus acts as a second barrier to transport of particles from the ICP into the orifice itself.

These two phenomena combine to form a boundary layer between the plasma stream and the orifice. This boundary layer

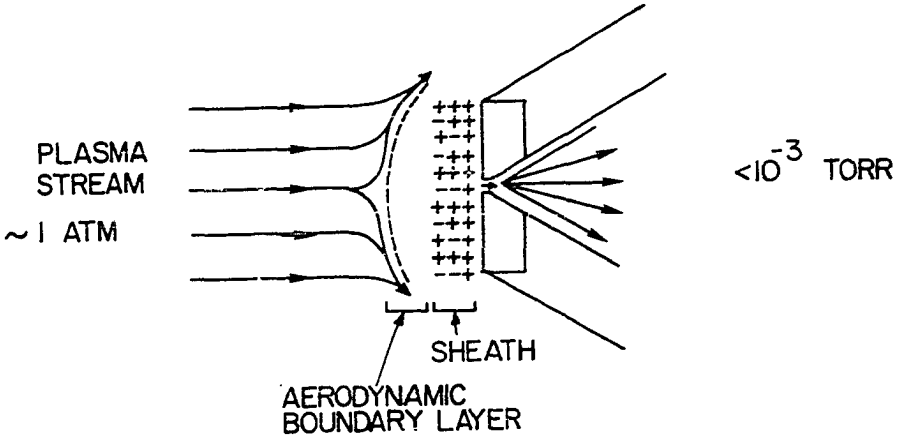

Figure 7a. Unbroken boundary layer. The gas flow through the orifice is insufficient to puncture the sheath and aerodynamic boundary layer.

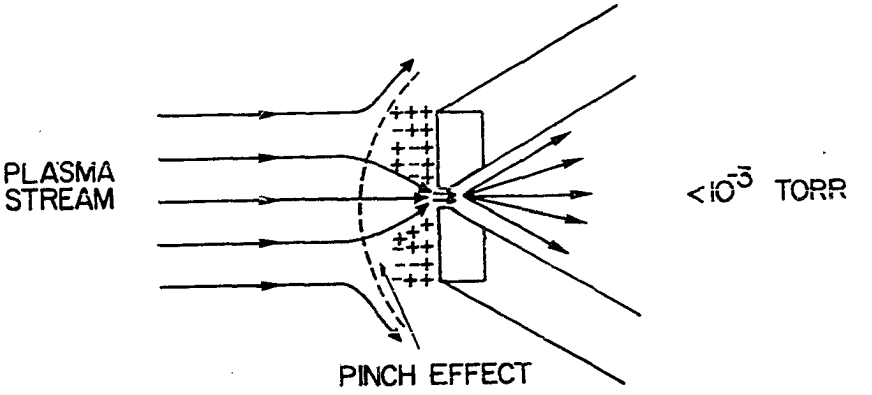

Figure 7b. Pinch effect. The gas flow through the orifice breaks through the sheath and aerodynamic boundary layer.

still near atmospheric pressure, providing ample opportunities for reactive collisions, including those involving positive ions or metastable argon atoms. A variety of ion-neutral, recombination, or metastable-induced reactions are therefore expected in the boundary layer. If the rates of these reactions are rapid relative to the rate at which the plasma constituents are sampled through the orifice, the ions extracted through the orifice would be representative of the boundary layer reactions rather than the plasma stream populations. Equation (14) approximates the aerodynamic contribution δ_A to the boundary layer thickness for a flat plate immersed in a flame or laminar flowing plasma of cross sectional diameter D.

$$\delta_A = 3\left(\frac{\nu D}{2v_0}\right)^{\frac{1}{2}} \qquad (14)$$

For the ICP ν = kinematic viscosity (cm^2/s) of argon at the plasma temperature, and v_0 = laminar flow velocity (cm/s) of the plasma region opposite the sampler tip, i.e., the axial channel. A residence time of 3 ms has been estimated for an analyte particle travelling through the axial channel (approximately 30 mm long) of an ICP in a standard torch. Thus v_0 = 1-1.5 x 10^3 cm/s at 1.0 L/min aerosol flow rate (103).

The temperature dependence of the kinematic viscosity is estimated as follows (104, 105).

$$\nu = \eta/\rho = \frac{\bar{c}\lambda}{3}$$

$$= \frac{1}{3}\left(\frac{8kTN_0}{\pi M_{Ar}}\right)^{\frac{1}{2}} \quad \frac{RT}{\sqrt{2}\pi\sigma^2 PN_0}$$

$$\nu(cm^2/s) = 2.35 \times 10^{-20} \frac{T^{3/2}}{\sigma^2} \text{ (CGS units)} \tag{15}$$

In these equations η = gas viscosity (poise), ρ = gas density (g/cm^3), $\bar{c}$ = mean particle thermal velocity (cm/s), λ = mean free path (cm), M_{Ar} = atomic mass of argon = 40 g/mole, R = ideal gas constant, and P = 1 atm. The collision diameter is estimated to be the van der Waals diameter of an argon atom, σ = 3.8 Å = 3.8×10^{-8} cm (106).

$$\nu(cm^2/s) = 1.63 \times 10^{-5} T^{3/2} \tag{16}$$

Because the cross-sectional diameter of the blunt tip of the sampler cone (Figure 6) is smaller than the axial channel diameter, D = tip "diameter" = 4.8 mm. Substitution of these values of D, v_0, and Equation (16) into Equation (14) gives the aerodynamic contribution to the boundary layer thickness.

$$\delta_A(mm) = 1.9 \times 10^{-4} T^{3/4} \tag{17}$$

For T = 4000-8000 K, δ_A = 1-1.6 mm; this range of values agrees approximately with the boundary layer thickness (approximately 1 mm) observed during ICP sampling (100).

Figure 7a shows an additional contribution to the total boundary layer thickness caused by the formation of an electrostatic sheath of thickness δ_S between the aerodynamic layer and the orifice disk. The sheath thickness should increase as the sampler potential (V_S) becomes more negative relative to the plasma potential (107-111).

An estimate of δ_S for ICP sampling is obtained from values observed for flame sampling. The following expression for sheath thickness is obtained from the data of Clements and Smy for a DC biased, cylindrical electrostatic probe immersed in an atmospheric pressure flame at ground potential (110).

$$\delta_S(\text{mm}) = b\left(\frac{v_0 V_S^2}{n_e D T_e}\right)^{1/4} \qquad (18)$$

In Equation (18), b is a proportionality constant calculated from their experimental determination of sheath thickness. At V_S = sampler voltage relative to flame = -300 volts, δ_S = 0.6 mm for their flame and probe (T_e = electron temperature = 2000 K, n_e = 1 x 10^{12} cm^{-3}, D = probe diameter = 5.0 cm, v_0 = 300 cm/s).

The DC potential of the ICP is uncertain. To be strictly comparable to this flame, the DC potential of the ICP would have to be +300 volts relative to the grounded sampler. Therefore, δ_S calculated as if the ICP actually operated at +300 volts DC undoubtedly represents a maximum value of sheath thickness (110). At constant V_S (relative to the plasma), Equation (18) can be simplified.

$$\delta_S(\text{mm}) = b' \left(\frac{v_0}{n_e D T_e^2} \right)^{1/4} \tag{19}$$

According to the data of Clements and Smy and Equation (19), $b' = 9600$; this proportionality constant is assumed to be similar for ICP sampling. From Equation (19), an estimate of δ_S is obtained for ICP sampling for $T_e = 7000$ K, $n_e = 5 \times 10^{14}$ cm^{-3}, $v_0 = 1000$ cm/s, and $D = 0.5$ cm. These values correspond to a sheath thickness of $\delta_S = 0.15$ mm during ICP sampling, which is approximately 15% of the total boundary layer thickness observed in the present work.

This estimate of the relative thickness of the aerodynamic and electrostatic boundary layers is supported by the following experimental observation. The total boundary layer thickness decreases drastically as the cross-sectional diameter of the blunt sampler tip decreases. The boundary

layer is thin enough to be indistinguishable for a sharply pointed tip. This thinning effect, i.e., boundary layer thickness decreases for more streamlined cone tips, clearly suggests an aerodynamic mechanism for boundary layer formation (35, 44, 101). Thus, the aerodynamic disturbance to gas flow makes the dominant contribution to the total boundary layer thickness.

If the sampler potential (ground) is equal to or less than the plasma potential, then the electrostatic sheath must form next to the sampler. The aerodynamic boundary layer then forms on top of the sheath, as shown in Figure 7a. Although the electrostatic sheath is relatively thin, its composition differs drastically from that of the flowing plasma, i.e., the sheath is essentially all ions and neutrals with no electrons. The sheath thickness may correspond to several mean free paths, which implies that plasma ions undergo collisions while diffusing through a region of positive space charge. The possible effects of such collisions on the extracted ions are unclear. Therefore, efforts are continuing to measure or fix the DC potential of the ICP in order to determine if a potential difference between plasma and sampler has any effect on ion extraction conditions in general.

For orifice diameters of 25-100 um (as are generally used with atmospheric pressure sources), a small fraction of

the plasma gas streams through the boundary layer and sampling orifice under continuum flow conditions (34, 37, 44). This sampling process is likely to occur in one of two modes (29, 35). If the flow into the orifice is insufficient to puncture the boundary layer (Figure 7a), the boundary layer extends unbroken across the orifice, and ICP particles undergo collisions with boundary layer species as previously described. The possibility then exists that boundary layer reactions could perturb the composition of the sampled gas. If the flow into the orifice punctures the boundary layer (Figure 7b), the ICP particles are drawn more directly into the vacuum system. Under the latter conditions, the composition of the sampled gas stream should approximate that of the plasma stream, i.e., ion populations should be closer to those prevalent in the plasma stream than when the boundary layer remains unbroken.

Two further opportunities for reactive collisions occur as ions, electrons, and neutral species from the plasma stream are drawn through the boundary layer and orifice. First the metallic wall of the orifice provides a hot metal surface in close contact with the gas stream, which could catalyze reactions in the sampled gas (35, 43). The average number of wall collisions is reduced by keeping the orifice diameter/length ratio as large as possible. Second, as the sampled gas leaves the orifice it forms a supersonically ex-

panding jet. Reactive collisions and scattering are commonly observed in molecular beam sources if the pressure in the expanding jet is too high. If the pumping speed is sufficient as the gas enters the vacuum system, the pressure falls rapidly to $\leq 10^{-3}$ torr and collision induced reactions become negligible (36, 44). The particles in the expanding jet are also cooled significantly by the end of the expansion process.

Once collisionless conditions are obtained, the positive ions in the expanding jet are collected, focused, and transmitted toward the mass spectrometer by an electrostatic ion lens. The unwanted electrons and neutral species are pumped away. The interface thus forms a beam of positive ions, some of which are characteristic of the trace elements in the solution aerosol being injected into the ICP.

Ideally, the interface should provide maximum ion transmission, reproducible analytical performance, and ease of operation. Clearly the largest orifice diameter (consistent with pumping speed) should yield maximum ion transmission and least susceptibility to orifice plugging by condensed solids from the plasma stream. Several other design factors are also relevant. The voltage difference between the plasma stream and the sampler should be externally variable, which may serve to control the plasma sheath thickness. The complicating reactions at each stage of the extraction

process should be either absent or controllable. The sampler should be at an elevated temperature, thereby minimizing solid condensation, aperture plugging, and memory effects. The orifice disk should be dimensionally stable during exposure to the ICP. Also, ion extraction should occur from a spatially finite region of the ICP so that spatial profiling is possible. These factors have been considered in developing the interface described below.

Conical skimmer

A water-cooled, stainless steel skimmer cone with a 4.6 mm diameter, knife-edged hole was centered on the plasma stream as shown in Figure 8. The hole diameter and outside taper were chosen to admit all of the axial channel portion of the ICP and to deflect the outer portion of the plasma stream outside the cone. Gases in the axial channel region of the ICP flowed through the skimmer hole, forming a well-defined plume. During nebulization of solutions with intensely emitting analytes such as sodium, the plume showed the corresponding color emitted by the excited atomic species. Entrainment of air into the plume became evident only 2 cm downstream from the skimmer tip. For example, during injection of an aerosol containing yttrium, the familiar blue, football-shaped region (corresponding to the emission of Y atoms) was observed in the plume for a few centimeters

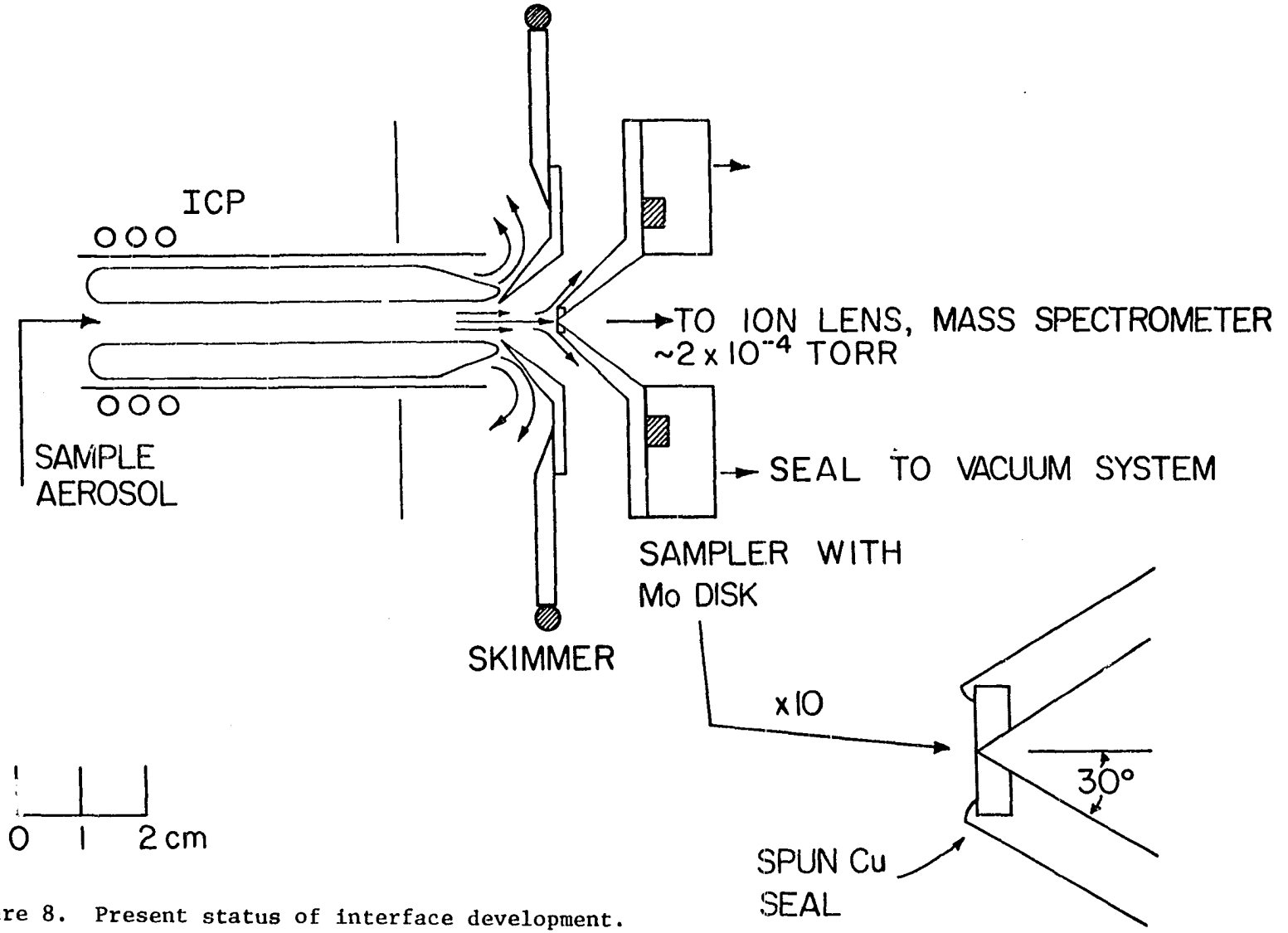

Figure 8. Present status of interface development.

downstream. This localized region was followed by a diffuse red "tail" caused by the band emission of YO, which was formed as air became entrained further downstream in the plume (76).

The skimmer was grounded through the inductive-capacitive (LC) filter shown in Figure 9. The filter effectively decoupled DC biased or grounded metal objects immersed in the ICP, reduced electrical noise levels due to RF interference, and promoted stable operation of the skimmer.

The skimmer was machined from a solid piece of stainless steel. Because of its poor thermal conductivity, the skimmer glowed orange-hot during exposure to the ICP. The elevated skimmer temperature (approximately 1000 K) greatly reduced the tendency of solids derived from analyte solutions to condense on either the skimmer or sampler tip. When such condensation occurred, ion sampling was unstable and the ICP frequently arced to the skimmer and sampler.

Sampler

After passing through the skimmer, the axial channel plume of the ICP, still near atmospheric pressure, encountered the sampler. The latter consisted of a water-cooled copper cone, tipped by a molybdenum disk with a 50 um diameter orifice drilled through the center of the disk. A small fraction of the plume gas, along with its ions, was

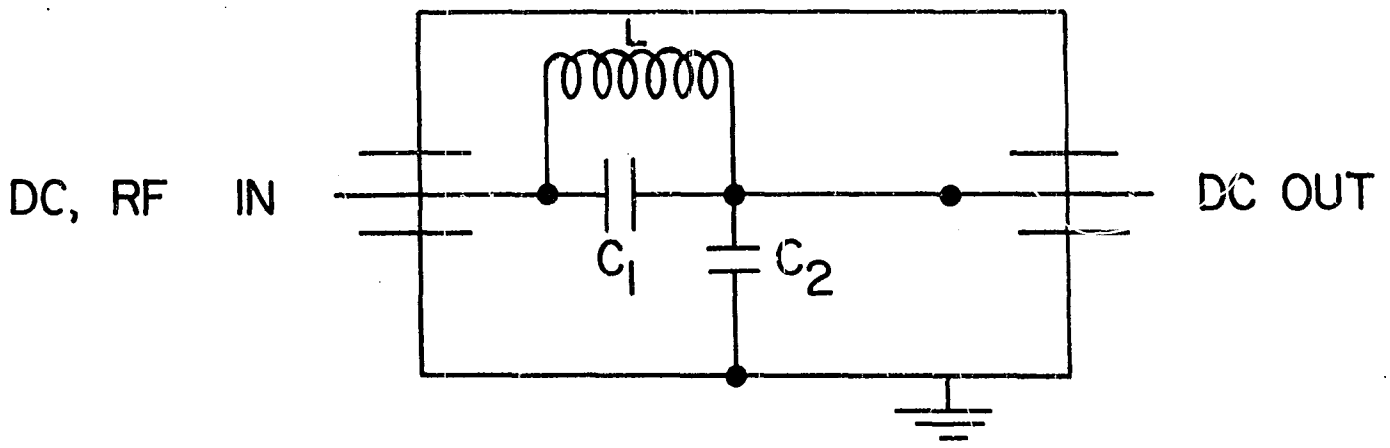

Figure 9. LC filter for reduction of RF interference. L = 3 mH, C_1 = 10-20 pF, C_2 = 1000 pF. Filter input is connected to grounded or biased object in or near ICP; filter output is connected to ground or DC voltage supply.

extracted under continuum flow conditions through this orifice into the first stage of a differentially pumped vacuum system, which housed an ion lens and quadrupole mass spectrometer.

During exposure to the ICP plume, the tip of the sampler cone was red hot (approximately 800 K). Again, the elevated temperature greatly reduced condensation of solids on the sampler tip and on the orifice disk. The base of the sampler was mounted on a water-cooled copper flange, which provided efficient heat transfer from the sampler tip. A typical sampler assembly operated in a stable fashion for nebulization of dilute (<100 ug/mL) analyte solutions for 8 to 10 hours before sampling conditions deteriorated due to gradual condensation of solid. The sampler was readily cleaned by immersing it in an ultrasonic water bath for a few minutes. An individual sampler remained useful for a total of approximately 100 hours. During this time the disk gradually became pitted and discolored and the orifice developed an irregular cross-section.

A Teflon gasket and Nylon bolts were used to connect the cooling flange to the vacuum system and to isolate it electrically from the vacuum system. The sampler cone was then grounded through another LC filter. This grounding scheme caused a greater reduction of RF interference in the ion gauges, counting electronics, and recording equipment

than was the case if the sampler was grounded directly to the vacuum system.

The ICP-skimmer assembly was mounted on a set of (x, y, z) linear translation stages (Ames Laboratory construction), which enabled movement of the plume relative to the sampler. Maximum count rates for analyte ions were obtained when the sampler tip was centered on the plume and thrust inside the skimmer approximately 2 mm behind the skimmer tip.

For an orifice disk with a 50 um hole diameter, the gas flow through the orifice was insufficient to puncture the remaining boundary layer (Figure 7a). The boundary layer could be punctured (as shown in Figure 7b) by employing a sharply pointed conical tip with a 50 um orifice (29, 35, 43, 44, 101); the sharp tip minimized the aerodynamic contribution to the boundary layer thickness, so that a 50 um orifice extracted enough gas to puncture the boundary layer (35, 44). This puncturing of the boundary layer was accompanied by the formation of a white-hot, funnel-like streamer of gas into the orifice. A flat orifice disk with a 70 um orifice also extracted enough gas from the ICP to puncture the boundary layer (Figure 7b). This extraction mode with a punctured boundary layer is called the "pinch effect". A similar "pinch effect"" is observed through the exit orifice of a duoplasmatron ion source (112, 113).

The "pinch effect" mode of sampling is desirable for several reasons: a) because the boundary layer is punctured, the sampled ion populations are likely to be more representative of the corresponding populations in the plasma (35, 44), b) the high temperature of the pinched plasma flow inhibits solid condensation at the orifice, and c) a 70 um orifice samples twice as much gas as a 50 um orifice and thus should result in the extraction of at least twice as many ions.

Unfortunately, the "pinch effect" causes a serious experimental difficulty. The high temperature of the constricted flow of plasma gases leads to unacceptably fast (<15 minutes) erosion of the orifice for all orifice assemblies tested so far. This erosion is not observed for similar orifice assemblies and extraction conditions with the CAP (69-73) or with a flame as an ionization cell (34-36, 43). Both of the latter VAEI cells have electron number densities that are 2 to 4 orders of magnitude below the values prevalent in the ICP (approximately 10^{15} cm^{-3}) (79). The "pinch effect" concentrates these electrons when all the particles from a cross sectional area of approximately 700 um diameter stream into a 70 um orifice. Also, because the "pinch effect" breaks through the boundary layer, the sampled gas is not significantly cooled by the orifice assembly before extraction. The conditions in the "pinched" gas are somewhat analogous to those in a constricted arc discharge

(also called a plasma jet), in which a radial constriction of the arc increases the number density and flow of the charged particles. The input energy is thus concentrated into a smaller volume, resulting in higher gas temperatures (114, 115). During extraction of ions from the ICP in the "pinch effect" mode, the enhanced temperature and electron number density adjacent to the orifice intensely heated the thin metal comprising the edge of the orifice. The edge of the orifice melted, and the fused metal then tended to flow down the inside contour of the sampler, where solidification occurred. The erosion continued until the hole expanded to a diameter that could not be tolerated by the vacuum system (≥150 um). Useful mass spectra have not been obtained during pinch effect sampling, hence this sampling mode was not used in the present work.

A physically durable sampler was constructed by recessing a metal disk with a 50 um orifice behind a retaining copper lip (inset on Figure 8) as previously described. The copper lip served as a vacuum seal, insured good thermal contact between the orifice assembly and the cooled cone, and caused a relatively thick boundary layer to form in front of the orifice. With proper balance between orifice diameter and boundary layer thickness, continuum flow into the orifice was insufficient to break through the boundary layer, and the "pinch effect" was prevented. The bounda-

ry layer thus shielded the pinhole from the fatal consequences of the "pinch effect", and yielded useful orifice lifetimes. The results presented below were obtained with the boundary layer sampling mode despite the complicating reactions that undoubtedly occur in this layer. The interface described here should therefore be considered as being in the developmental stage. Further improvements in its performance are expected. In particular, it should be possible to develop an orifice assembly which can physically withstand the "pinch effect", thus greatly reducing the potentially undesirable effects of boundary layer reactions.

Vacuum System, Gas Extraction Rate, and Pumping Speed

The sampler cone and orifice assembly were mounted on a two stage, differentially pumped vacuum system of welded stainless steel construction. The first stage (Figure 10) was evacuated by a 1600 L/s oil diffusion pump (Lexington Vacuum Division, Varian Asociates, Lexington, MD). The electrostatic ion lens was mounted in the first stage. As shown in Table I, the first stage pressure (measured by a Pirani gauge) was sufficiently low for ion collection and beam formation but too high for mass spectrometer operation. A second stage of differential pumping was therefore required. The ions were directed through a 3 mm diameter x 8 mm long

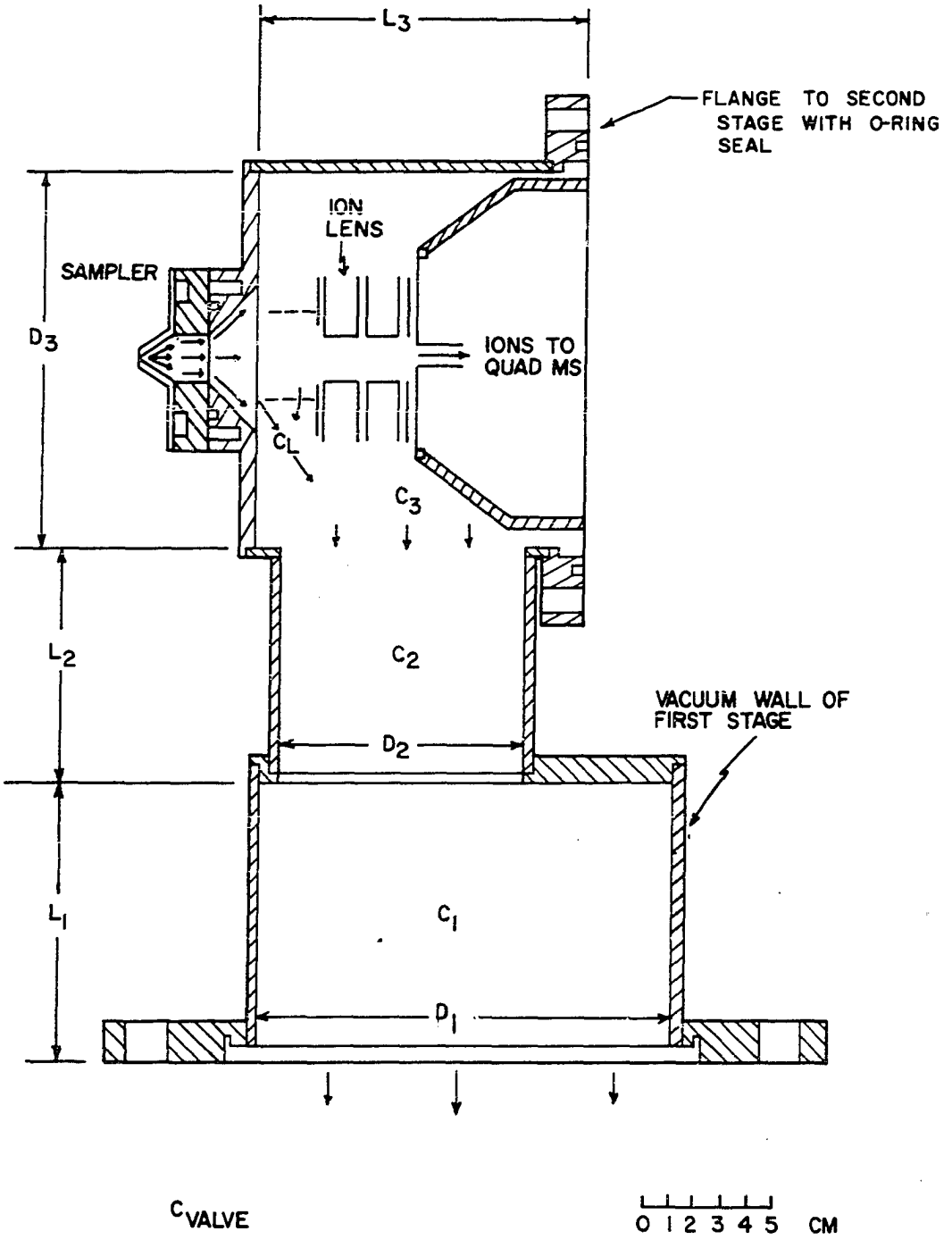

Figure 10. First stage of differentially pumped vacuum system.

aperture into the second stage, which housed the quadrupole mass spectrometer. The second stage was pumped by a second 1600 L/s oil diffusion pump equipped with a liquid nitrogen-cooled baffle. Both pumping stations were provided with slide valves to permit rapid venting for sampler installation or modification of internal components.

The conductance of the orifice C_{IN} under continuum flow conditions when sampling flame gases at 1 atm is given by Knewstubb (38).

$$C_{IN}\ (L/s) = 20\ A \tag{20}$$

$$A = \text{orifice area } (cm^2)$$

$$A = \frac{\pi d_{cm}^2}{4}$$

where d_{cm} = orifice diameter (cm). Equation (20) is used to approximate the conductance of the orifice for sampled plasma gas. The throughput $Q_{IN} = P_{IN} C_{IN}$ for plasma gas pressure P_{IN} must equal the throughput of the first diffusion pump $Q_{PUMP} = P_V S_V$, where P_V and S_V = pressure and net pumping speed inside the vacuum system at the point where the supersonic expansion becomes collisionless. The first few millimeters of the cone interior are discolored, presumably due to wall collisions of extracted particles. This observation indicates that the

supersonic jet becomes collisionless somewhere further inside the vacuum system.

$$Q_{IN} = Q_{PUMP}$$

$$S_V = \frac{P_{IN}C_{IN}}{P_V} \tag{21}$$

In Equation (21), the effective P_{IN} = (760/2.5) torr = 304 torr, because the first stage pressure decreases by a factor of 2.5 for ICP sampling relative to air sampling (Table I). Combining Equations (20) and (21) gives a convenient expression for the net pumping speed of the vacuum system.

$$S_V(L/s) = 4780 \frac{d_{cm}^2}{P_V} \tag{22}$$

50 um orifice: $d_{cm} = 50 \times 10^{-4}$ cm

$P_V = 4 \times 10^{-4}$ torr

$S_V = 298$ L/s

70 um orifice: $d_{cm} = 70 \times 10^{-4}$ cm

$P_V = 8 \times 10^{-4}$ torr

$S_V = 292$ L/s

Thus a net pumping speed of approximately 300 L/s accounts for the pressure observed with both orifice diameters used in

the present work.

This net pumping speed is provided by a diffusion pump (S_{PUMP} = 1600 L/s) through a slide valve and a set of cylindrical tubes (Figure 10), which comprise the first stage of the vacuum system. They also restrict the conductance so that the full speed of the pump is not obtained near the sampling orifice. The net pumping speed S_V of a system with a pump of speed S_{PUMP} connected by a "tube" of equivalent conductance C_t is (116, 117):

$$\frac{1}{S_V} = \frac{1}{C_t} + \frac{1}{S_{PUMP}} . \tag{23}$$

The equivalent conductance C_t of i pipes connected in series is

$$\frac{1}{C_t} = \sum_i \frac{1}{C_i} , \tag{24}$$

where the conductance under molecular flow of the i'th pipe of diameter D_i (cm) and length ℓ_i (cm) is given below (116).

$$C_i = \frac{1}{6} \frac{D_i^3}{\ell_i} \left(\frac{2\pi k T_{ROOM} N_G}{M} \right)^{\frac{1}{2}}$$

$$C_i(L/s) = 10.4 \frac{D_i^3}{\ell_i} \tag{25}$$

Equation (25) holds for argon at 300 K with D and ℓ expressed

in centimeters. The dimensions and conductance of each tube are listed in Table II. If the lens were not present, the equivalent conductance and net pumping speed would be as follows.

$$\frac{1}{C_t} = \frac{1}{C_{VALVE}} + \frac{1}{C_1} + \frac{1}{C_2} + \frac{1}{C_3} \tag{26}$$

$$C_t = 573 \text{ L/s}$$

$$\frac{1}{S_V} = \frac{1}{C_t} + \frac{1}{S_{PUMP}}$$

$$S_V = 422 \text{ L/s}$$

This value of net pumping speed is above the measured speed, because the $1/C_3$ term in Equation (26) does not account for the restricted conductance around and through the ion lens. The corrected conductance C_3' of the third pipe is defined as some fraction a of its conductance if the lens were not present.

$$C_3' = aC_3$$

Substitution of the observed S_V and C_3' for C_3 into Equation (26) yields an estimate of a.

$$\frac{1}{S_V} = \frac{1}{C_{VALVE}} + \frac{1}{C_1} + \frac{1}{C_2} + \frac{1}{aC_3} + \frac{1}{S_{PUMP}}$$

$$a = 25\%$$

Thus the presence of the ion lens reduces the effective conductance of the third tube by approximately 75% and the net pumping speed by approximately 30%.

Table II. Parameters for Calculation of Pumping Speed of First Stage. Conductances are Calculated for Argon at 300 K.

COMPONENT (subscript i)	D_i (cm)	ℓ_i (cm)	C_i (L/s)
VALVE	-	-	5530
1	16.2	11.1	4000
2	9.52	8.89	1010
3	14.6	10.5	3090

S_{PUMP} = 1600 L/s

Collisions During Extraction Process

During extraction the average residence time t, collision frequency f, and total number of collisions N_{COL} characteristic of particles in the stagnant region of gas between the ICP and orifice may be estimated as follows. For the idealized representation of the orifice assembly shown in

the inset of Figure 8, the volume v of the stagnant region may be approximated as the volume of the "disk" of gas in front of the orifice.

$$v = \pi r^2 h \tag{27}$$

where r = radius of orifice disk and h = height of the tip of the sealing copper lip above the orifice disk. For the 50 um orifice, $v = 6.3 \times 10^{-7}$ L. This volume is pumped through the orifice of conductance C_{IN} given by Equation (20), i.e., $C_{IN} = 3.9 \times 10^{-4}$ L/s. The particles in the stagnant layer are enclosed there by the copper sealing lip. These trapped particles are eventually pumped through the orifice. Thus, the average residence time t is approximated by the time taken to pump one increment of gas equal to the volume of the stagnant region through the orifice, i.e.,

$$t = v/C_{IN} \qquad t = v/C_{IN}$$

For the 50 um orifice, t = 0.002 s.

The collision frequency f in the stagnant region is estimated as follows (105).

$$f = \sqrt{2}\, \pi \sigma^2 \bar{c}\, n \tag{28}$$

where n = total particle number density (cm^{-3}), $\bar{c}$ = mean thermal velocity (cm/s), and σ = 3.8 Å = 3.8 x 10^{-8} cm is the collision diameter. Although Equation (29) is strictly valid only for collisions between like particles in a homogeneous gas, it should provide a reasonable estimate of f because the plasma is nearly all argon. The following substitutions enable calculation of f.

$$\bar{c} = \left(\frac{8kT_{ICP}N_O}{\pi M} \right)^{\frac{1}{2}}$$

$$n = \frac{N_O(1\ atm)}{RT_{ICP}}$$

$$f \approx \frac{10^{11}}{\sqrt{T_{ICP}}}\ \text{collisions/s} \qquad (29)$$

The average temperature of the stagnant region should be between the ICP (approximately 6000 K) and the cone tip (approximately 800 K), at which temperatures f = 1-3 x 10^9 collisions/sec. Therefore N_{COL} is calculated as follows (94).

$$N_{COL} = (ft)/2 = 1\text{-}3 \times 10^6 \text{ collisions}$$

The stagnant region thus provides plentiful opportunities for collisions before extraction.

Electrostatic Ion Lens System

Because of the need for efficient pumping in the first stage, the differential pumping aperture leading to the mass spectrometer is located approximately 10 cm from the orifice. An electrostatic ion lens system collects, focuses, and transmits positive ions from the outer edge of the supersonic jet to the mass spectrometer. As shown in Figure 1, the electrostatic ion lens system consisted of a set of coaxial, sequential cylinders, each biased at a particular DC voltage. Maximum ion signals were obtained at the voltages specified in Table I. The shapes, width, resolution, and symmetry of the ion peaks were unaffected by the voltage settings on the ion optical elements, indicating that the energy spread of the ions was independent of the voltage settings on the lens elements. The cylindrical section of the first element was made of stainless steel screen (#16 mesh) to provide fast pumping of neutral species from the ion collection and collimation region. A 4.6 mm diameter solid metal disk was positioned in the center of the first element. This disk acted as an optical baffle, i.e., it blocked the line of sight from the ICP through the sampler orifice, lens system, and quadrupole axis and thus helped to prevent photons from the ICP from reaching the electron multiplier.

The motion of charged particles under the influence of an external electric field under collisionless conditions is described by the Laplace Equation. A set of sequential, conducting cylinders at different potentials can exert a focusing action on the charged particles. The set of cylinders is thus termed an ion lens, whose focusing action is derived from the curvature of the equipotential surfaces in the region between the cylinders. An ion lens is characterized by ion optical parameters such as focal lengths, magnification factors, and aberration coefficients that are closely analogous to their counterparts in light optics. Ion optical parameters can be calculated and measured by a variety of techniques (118-130). The ion optical parameters for a particular arrangement of lens elements, i.e., the cylinders in the present apparatus, can be changed by varying the applied voltages. This built-in adjustment is fortunate, because the electrode geometries and voltages used in the present work do not correspond to a configuration for which either calculated or measured lens parameters are available. Therefore, the following summary of lens performance is based mainly on empirical observations.

Characteristic curves of ion signal as a function of lens voltages are shown in Figure 11. The ion signal was measured in one of two ways: a) as a total ion current signal at a faraday cup mounted just inside the second stage behind

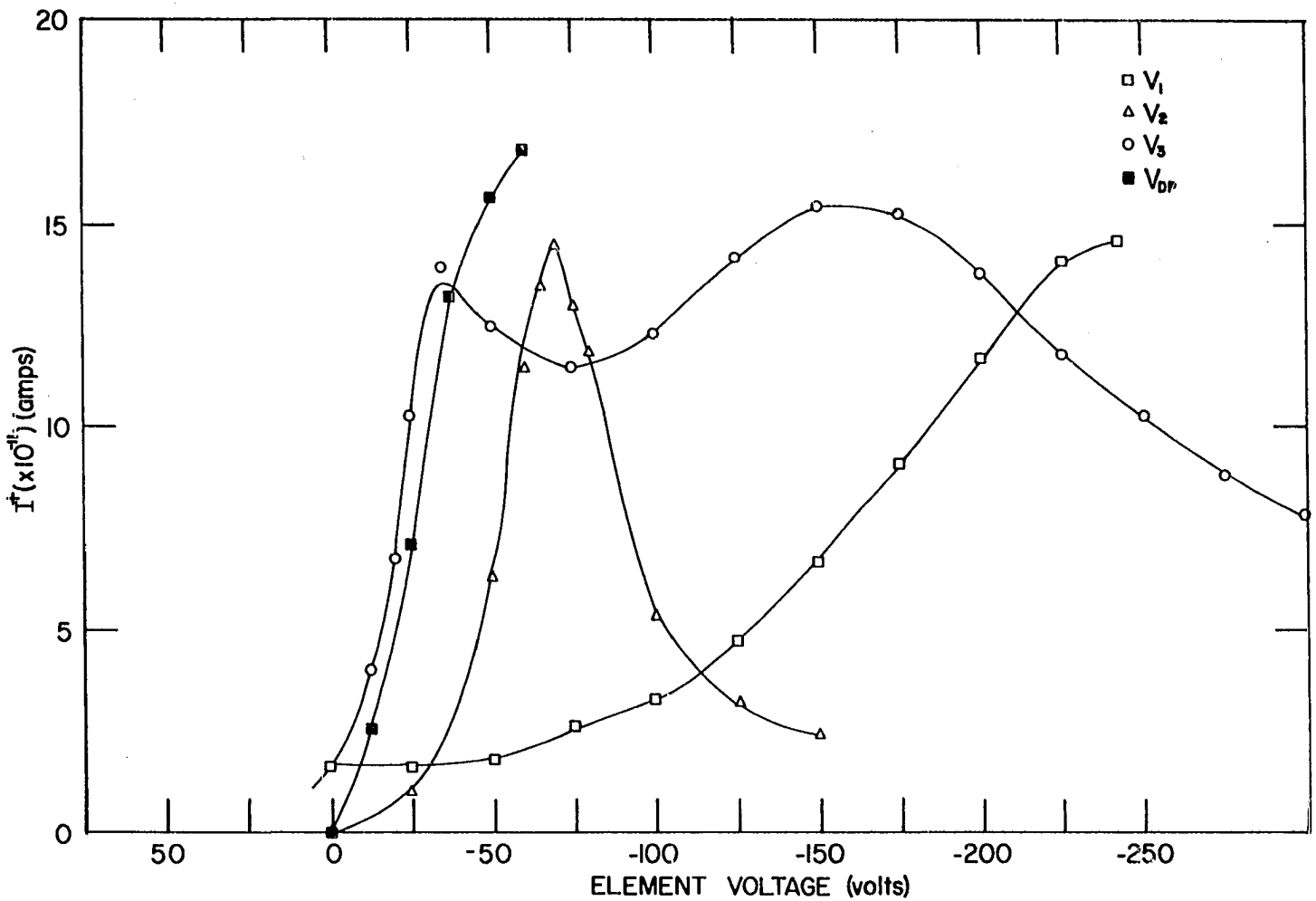

Figure 11. Characteristic curves of total ion current versus voltage of individual lens elements (Figure 1). As one voltage was varied the other voltages were left at their optimum values (Table I).

the differential pumping aperture, or b) as a mass-resolved ion count rate at the detector of the mass spectrometer. As the ions clear the "gas drag" effects of entrainment in the supersonic jet, the potential at that point becomes the effective ion energy (59). The apparatus was generally operated with the sampler grounded (V_S=0); thus, the ions are cut off for $V_{DP} > 0$ V in Figure 11. Also, a DC voltage ($V_S \neq 0$) could be applied to the sampler through an LC filter (Figure 9) and DC voltage supply. For a positive voltage on the sampler ($V_S > 0$), the ions are cut off at $V_{DP} \geq V_S$ (Figure 12), providing further evidence that the effective ion energy is the voltage at the point inside the sampler cone where the supersonic jet becomes collisionless. Apparently a positive voltage on the sampler does not inhibit extraction of ions. Thus the ions are extracted primarily by entrainment in the continuum flow through the orifice. Once inside the vacuum system, a positive voltage on the cone repels positive ions toward the ion lens, causing the ions to be collected, focused, and transmitted more efficiently. The sampler cone can thus function like the "ion box" of an electron impact source. From an ion optical standpoint, the ions are "formed" at the sampler voltage. Also, the positive voltage should attract electrons, possibly removing them and thereby inhibiting ion-electron recombination in the supersonic jet. This "biased sampler" mode, i.e., $V_S > 0$,

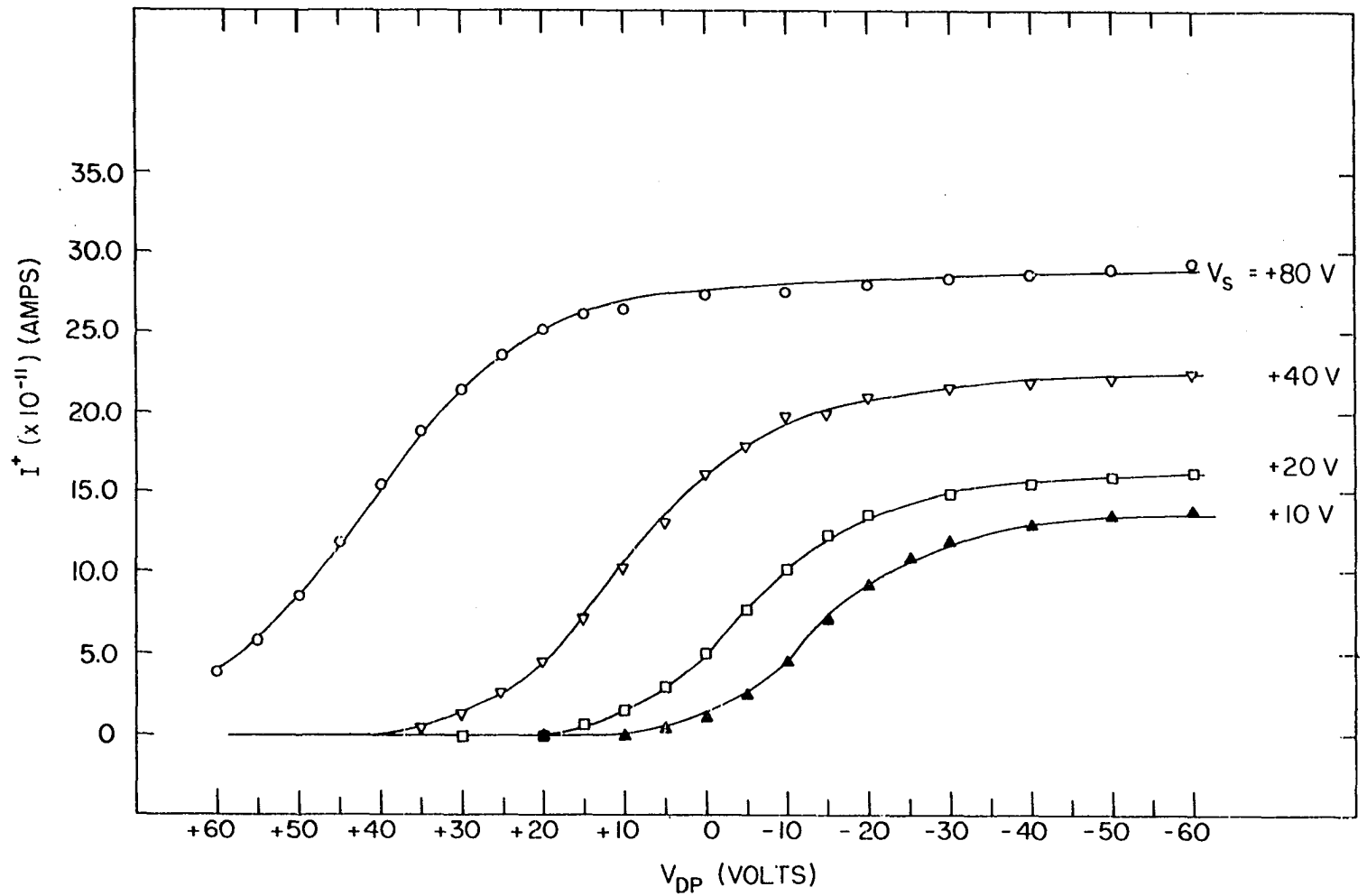

Figure 12. Total ion current as a function of voltage on the differential pumping aperture (Figure 1).

was not extensively used in the present work because it was generally accompanied by excessive noise due to RF interference in the ion gauges and recorder. Figure 12 indicates that it should be possible to increase the transmission by biassing the sampler above ground provided the RF interference can be eliminated and the ion optical requirements of the quadrupole, e.g., energy spread and residence time in the field region, are satisfied.

Positive ions are attracted toward the first cylinder (V_1) while electrons are repelled and neutral species are pumped away. Thus, the first cylinder acts as a "draw out" electrode in that it a) collects positive ions from the supersonic jet, b) prevents them from being pumped away, and c) keeps them moving toward the mass analyzer. This "draw out" function of the first lens element is substantiated by Gray and Hayhurst, who also observed a broad hump with a maximum at approximately -200 V in the characteristic curve for the first lens element for a variety of electrode sizes and shapes (33, 34, 69, 70).

The potential gradient region between the first and second cylinders apparently provides the strongest focusing action because of the sharp peak in the characteristic curve for V_2. The broad humps observed in the characteristic curves for the other ion optical elements (V_3-V_{DP}) indicate that their main function is transmission rather than focusing

of ions.

The present ion lens system may be one of the least effective components of the ICP-MS system. For example, fragmentary observations made with and without the optical baffle indicate that the baffle may cut off up to 80% of the ions. Also, the front surfaces of the first cylinder and differential pumping element become highly discolored after extensive use, which indicates that a significant number of ions strike these elements rather than moving into the second stage. Clearly, a more detailed experimental and/or mathematical investigation of this ion optical problem is warranted in future development of the ICP-MS technique.

Mass Analyzer

The quadrupole mass analyzer (originally supplied as a residual gas analyzer) was modified as follows. First, the filaments, grid, and reflector of the electron impact ionizer were removed; the focus plate was retained as the quadrupole entrance aperture. The latter was aligned visually with the center of the lens system by shimming under the rod mounting bracket. Second, the rods were biased below ground by connecting separate DC supplies into the DC rod driver circuit. As described in the last section, the initial ion energy was 0 V. Application of a negative DC bias to the

rods helped draw ions through the field region, thus improving their transmission. The mass spectrometer had a mass range of 1-300 u with resolution sufficient to resolve adjacent masses unless one peak was much more intense than the adjacent one. Because the transmission of the mass spectrometer dropped significantly as the transmitted mass increased, the observation of relatively low analyte masses was emphasized in this feasibility study.

The availability of simple, versatile, and fairly inexpensive quadrupole mass analyzers has contributed to the explosive expansion of mass spectrometry as a measurement technique for a variety of applications. The theoretical and practical aspects of the operation of quadrupole mass analyzers have been described (131-136). A quadrupole instrument is particularly suitable for mass analysis of ions extracted from a plasma for several reasons. First, the relatively high operating pressure ($\leq 5 \times 10^{-5}$ torr) tolerable to a quadrupole reduces the pumping speed required of the vacuum system. This property also enables the use of large slits or apertures between stages, thus enhancing the number of ions that can be transmitted into the second stage for mass analysis. Second, the resolution and transmission attainable with a quadrupole are rather insensitive to the component of ion velocity parallel to the quadrupole axis. Also, the transmitted m/z value increases linearly with the

DC and RF voltages applied to the rod structure. Because of the ease and rapidity with which these voltages can be switched, mass programming is easy and versatile. Finally, the potential powers of detection are very high, especially with electron multiplier detection in a pulse counting mode.

There are three major disadvantages to the use of a quadrupole instrument in the present work. First, the resolution is generally insufficient to resolve chemically different ions at the same m/z value, e.g., $^{40}Ar^{+}\cdot H_2O$ and $^{58}Ni^{+}$. Thus a simple mass spectrum free of spectral interferences is a necessity for multicomponent determinations with a quadrupole instrument. Second, the transmission generally decreases as the transmitted m/z value increases. Most quadrupoles thus discriminate against heavy ions, as shown in Figure 13. Finally, only ions of one m/z value strike the detector in a certain time for given values of the DC and RF voltages. Thus, the quadrupole mass analyzer is inherently limited to sequential determinations. It can be scanned repetitively and very rapidly and the signal-to-noise ratio for multiple ion determinations increased by signal averaging techniques. The result is a rapid but still inherently sequential method for mass analysis in a multiple ion mode.

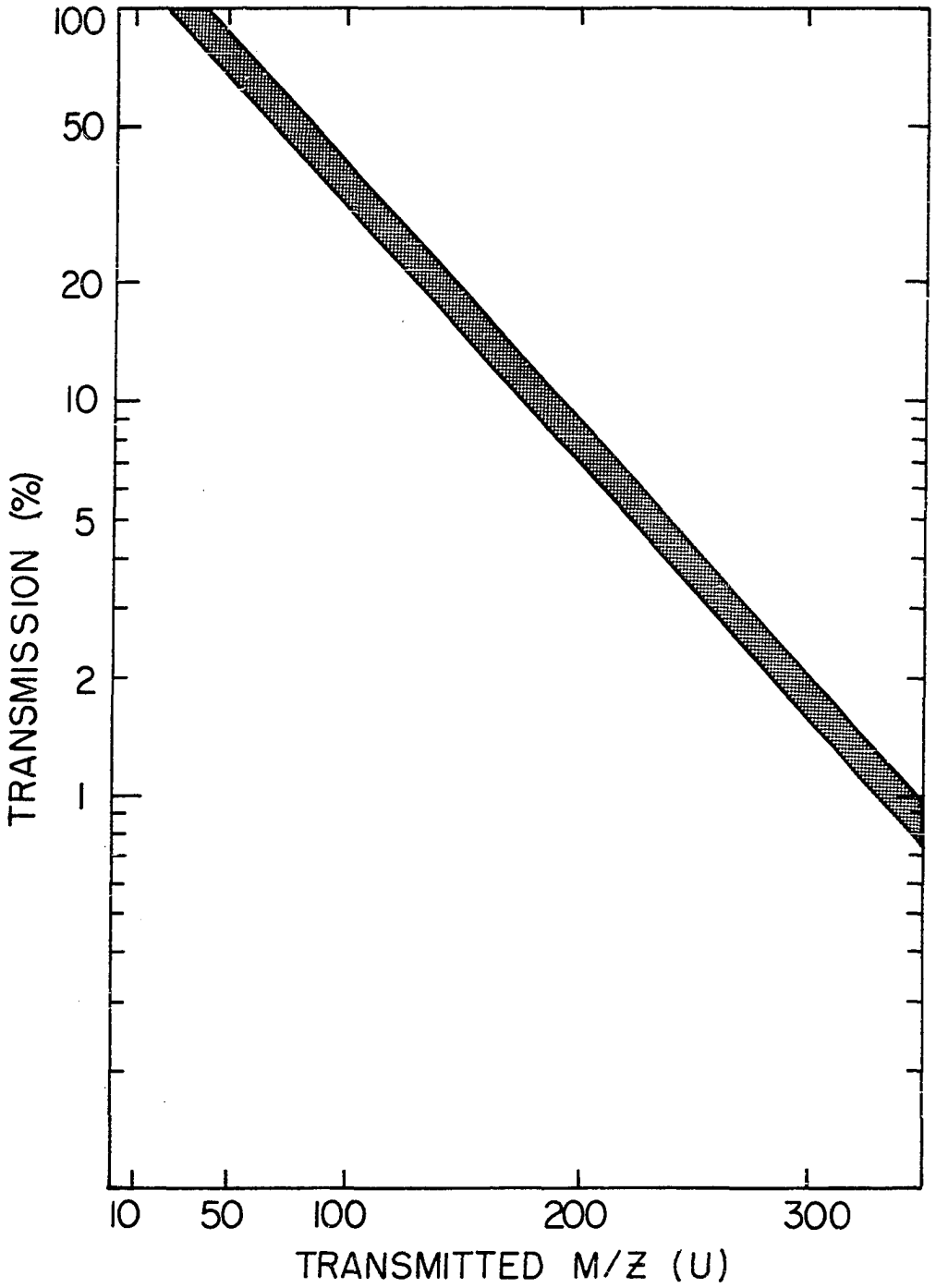

Figure 13. Mass discrimination curve supplied with UTI 100 C.

Electron Multiplier and Pulse Counting Electronics

The Channeltron electron multiplier (CEM) detector supplied with the mass spectrometer was operated in the pulse counting mode even though the multiplier was not saturated at a cathode bias of -4kV. Although this multiplier had a much lower gain than those designed specifically for pulse counting, it still performed adequately for the following reasons. First, there was no evidence of loss of gain or pulse overlap at count rates up to at least 5 x 10^4 counts/s. The multiplier therefore had a linear dynamic range of at least 5 x 10^4. Second, there was no indication of a chemical or mass effect on the multiplier efficiency (pulses out/ions in). Finally at -4kV the threshold setting on the pulse counting equipment could be set over a broad range (0.2-30 mV) without attenuating the observed count rate. The pulses were conducted from the multiplier anode to a preamplifier-discriminator-counter system. The counting threshold was set just above the height of RF noise pulses from the ICP.

The operating principles of a CEM have been described (137, 138). The CEM has several characteristics that make it desirable in the present application. First, it is suitable for pulse counting from the standpoint of pulse height distribution, rise time, pulse shape, and dynamic range. The

dark current count rate is very low (<1 count/s). The CEM tolerates relatively poor vacuum conditions and repeated venting to atmosphere without rapid degradation of gain.

Mass Spectra, Analytical Calibration Curves, and Detection Limits

The reference blank solution and the matrix for the reference solutions used for calibration consisted of 1% (vol.) nitric acid, prepared by diluting doubly distilled, concentrated nitric acid with deionized water. The reference calibration solutions were prepared by appropriate dilution of stock solutions. The stock solutions were prepared by dissolving pure metals or reagent grade salts in dilute nitric acid.

Mass spectra were acquired in the scanning mode as described in Table I. Individual points for analytical calibration curves were obtained in the single ion mode. The average total count for the reference blank solution at the mass of interest was evaluated first, followed by the average total count for each reference calibration solution, in ascending order of concentration. The average total count for the reference blank was then subtracted from the average total count for each reference standard solution before plotting. The detection limit was calculated as the analyte concentration required to give an average net count equal to

twice the standard deviation observed at the mass of interest for the blank solution, $2\sigma_b$.

The single ion data were punched in a specific format onto paper tape. The paper tape contents were then transferred to disk storage at the ISU Computer Center and edited by WYLBUR. The averaging, background subtraction, detection limit calculation, and analytical calibration curve plotting was then performed by a PL/1 program. The ionization energies and relative abundances of naturally occurring isotopes of the elements studied in the present work are listed in Table III for future reference.

Table III. Ionization Energies and Relative Abundance of Naturally Occurring Isotopes of Elements Studied.

ELEMENT	IE (eV)	MASS (u)	RELATIVE ABUNDANCE (%)
Na	5.14	23	100.
Mg	7.65	24	78.70
		25	10.13
		26	11.17
Ar	15.76	36	0.337
		38	0.063
		40	99.60
Cr	6.77	50	4.31
		52	83.76
		53	9.55
		54	2.38
Mn	7.44	55	100.
Co	7.86	59	100.
Cu	7.73	63	69.09
		65	30.91
As	9.81	75	100.
Rb	4.18	85	72.15
		87	27.85
Y	6.38	89	100.
Ag	7.58	107	51.82
		109	48.18
Cd	8.99	106	1.22
		108	0.88
		110	12.39
		111	12.75
		112	24.07
		113	12.26
		114	28.86
		116	7.58

CHAPTER III. ANALYTICAL RESULTS AND DISCUSSION

The mass spectrum of the major positive ions from the ICP plume observed during nebulization of a reference blank solution (1% nitric acid) is shown in Figure 14. The two most intense peaks correspond to Ar^+ (40 u) and ArH^+ (41 u). A comparable peak for H^+ (1 u) is evident, with its low mass edge obscured by "zero blast", i.e., ions anomalously transmitted through the quadrupole field region at the beginning of a scan because the low applied potentials lead to very weak fields within the rod structure (133). The existence of an intense peak due to ArH^+, along with the observation of other cluster ions such as H_3O^+ (19 u) and Ar_2^+ (80 u) indicate that some clustering reactions occur during ion extraction. Some of the more probable reactions are:

$Ar^+ + H \rightarrow ArH^+$

$Ar^+ + H_2O \rightarrow ArH^+ + OH$

$H^+ + H_2O \rightarrow H_3O^+$

$H_2O^+ + H_2O \rightarrow H_3O^+ + OH$

$Ar^+ + Ar \rightarrow Ar_2^+$

Such reactions probably occur in the relatively cool boundary layer that blocks entry of the plasma into the orifice. The hot metal surface (approximately 600 C) of the orifice disk,

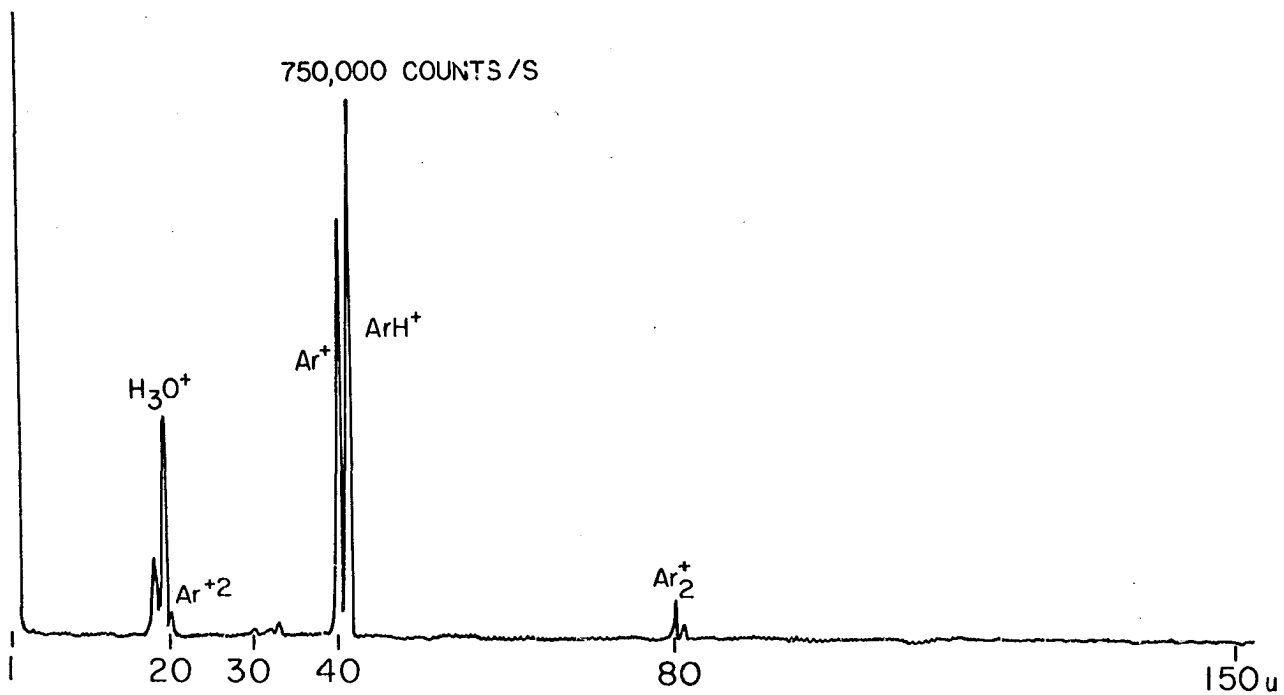

Figure 14. Positive ion mass spectrum of reference blank solution (1% HNO_3 in deionized distilled water). Vertical scale is linear with count rate; base peak (ArH^+) count rate indicated. Background ranged from 30-100 counts/s.

which is in close contact with the boundary layer, may catalyze such reactions (35, 43). In addition to reactions involving ions, the sharp temperature gradient between the ICP plume and the boundary layer may enhance the formation of metastable argon atoms (designated Ar^m) (82, 84, 85), thus providing additional highly reactive species in the collision-rich boundary layer. Ion-neutral reactions and Ar^m reactions leading to clustering may also occur just after extraction into the vacuum system. The pressure in the supersonically expanding jet of sampled gas remains high enough to allow numerous collisions until the particles have travelled several millimeters, providing further possibilities for clustering. Despite these sources of complicating reactions, the mass spectrum for the reference blank solution is relatively free of molecular ion spectral interferences.

The major and minor ions observed to date in the mass spectrum of the reference blank solution are identified in Table IV. No ions above 81 u were observed from the reference blank solution. All of the major ions and many of the minor ions have been observed previously by other investigators in the mass spectra of flames (25-27, 30-43, 45, 46) and plasmas (19, 22, 38, 47-49, 63-65, 69, 70) or as analogous cluster species formed during supersonic jet expansions (32, 35, 45). The major ion masses observed were identical for all of the samplers examined so far. However, the

absolute and relative count rates for the major ion peaks varied within a factor of 2 for different samplers (of similar construction) and from day to day for the same sampler. Greater variation (sampler to sampler and day to day) was observed for the absolute and relative count rates of the minor ions. As indicated in Table IV, not all of the minor ion species were detectable with each sampler, resulting in a fortuitous simplification of the mass spectrum of the reference blank solution. Apparently, subtle differences in the extraction conditions existed on different days and for different samplers. Fortunately, the count rates for the minor ions were small (≤1000 counts/s), and the entire spectrum of the reference blank solution was qualitatively and quantitatively reproducible for 5 to 10 hours. Subtraction of the reference blank spectrum thus provided adequate background correction at those masses corresponding to ions from most of the elements.

The count rate obtained for the reference blank spectrum at those masses free of major or minor ions was 30-100 counts/s, well above the dark current count rate characteristic of the electron multiplier (≤1 count/s). This background count rate was the same at all masses and was independent of the ion lens voltages and mass analyzer operating conditions. Apparently, this background was caused by vacuum UV photons striking the electron multiplier. These photons probably are

Table IV. Major and Minor Ions Observed in Mass Spectrum of Reference Blank Solution.

MAJOR IONS Mass	Ion(s)	Relative Count Rate	
		Ar^+=100	$^{55}Mn^+$=100
16	O^+	0.4	4
17	HO^+, NH_3^+	1	10
18	H_2O^+, NH_4^+	12	120
19	H_3O^+	40	400
20	Ar^{+2}	4	40
30	NO^+	4	40
32	O_2^+	2	20
33	$(O_2^+)\bullet H$	4	40
36	$^{36}Ar^+$	0.8	8
37	$^{36}ArH^+$ $(H_2O)\bullet H_3O^+$	1	10
40	$^{40}Ar^+$	75	750
41	$^{40}ArH^+$ $(Na^+)\bullet H_2O$	100	1000
80	Ar_2^+	8	80
81	$(ArH^+)\bullet Ar$	3	30

Table IV (continued)

MINOR IONS Mass	Ion(s)	Detected with all samplers?
14	N^+	Yes
21	$(Ar^{+2})\bullet H$	No
	$H_3{}^{18}O^+$	
28	N_2^+, $^{28}Si^+$	No
31	$(NO^+)\bullet H$	No
38	$^{38}Ar^+$	Yes
45	N_2OH^+	Yes
46	SiO^+	Yes
	NO_2^+	
47	$(SiO^+)\bullet H$	No
	$(NO_2^+)\bullet H$	
48	$(NO^+)\bullet H_2O$	Yes
50	$(O_2^+)\bullet H_2O$	Yes
54	$^{54}Fe^+$	Yes
	$(^{36}Ar^+)\bullet H_2O$	
55	$(H_3O^+)\bullet 2H_2O$	No
56	$^{40}ArO^+$	Yes
	$^{56}Fe^+$	
57	$^{40}ArOH^+$	Yes
58	$(^{40}Ar^+)\bullet H_2O$	Yes
59	$(^{40}ArH^+)\bullet H_2O$	No

Table IV (continued)

Mass	Ion(s)	Detected with all samplers?
60	?	No
68	?	No
69	?	No
71	?	No
73	$(H_3O^+) \cdot 3H_2O$	Yes
76	$(^{40}Ar^+) \cdot {}^{36}Ar$	Yes
77	$(^{40}ArH^+) \cdot {}^{36}Ar$	Yes

Possible ions at same mass number are listed in decreasing order of likelihood or probable intensity. ArH^+ = 750,000 counts/s; $^{55}Mn^+$ =75,000 counts/s at 50 ug/mL solution concentration. Minor ion count rates were always ≤ 0.4 relative to ArH^+ = 100.

radiated directly from the ICP and also from the decay of Ar^m within the vacuum system. Although the direct line-of-sight from the orifice through the quadrupole field region is blocked by a disk-like baffle (Figure 1) and the multiplier is offset from the quadrupole axis, numerous photons still strike the multiplier, generating the observed background level (30-100 counts/s). The background count rate at each mass of interest of the reference blank solution was reproducible during a 5 to 10 hour period, and single ion data for reference standards and samples were adequately corrected by subtraction of the reference blank as previously described. However, because the powers of detection are limited by the standard deviation of the background, it is highly desirable to minimize the photon background. Gray nearly eliminated the photon background in his study by tilting the plasma relative to the centerline of the vacuum system so that the quadrupole axis and multiplier were not in line with the photon source (69, 70). This angular extraction technique has not yet been applied in these ICP-MS studies.

The recorded peaks of monatomic, singly charged positive ions from solutions of Mn, Cu, Rb, and Ag are shown superimposed on the reference blank spectrum in Figure 15. The metal ion spectra are plotted on the same mass and count rate scales as the reference blank spectrum but are displaced vertically by a change in the recorder zero. As shown in the

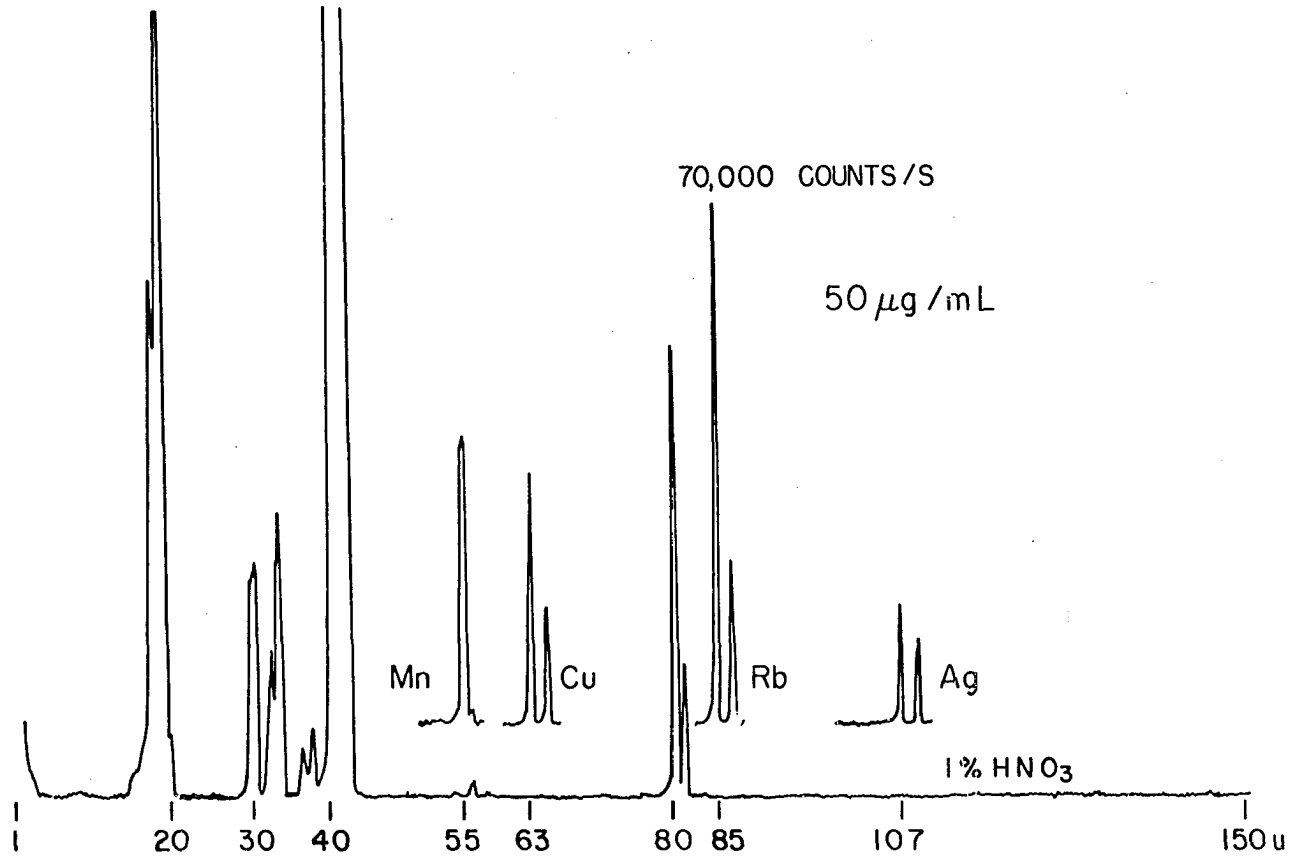

Figure 15. Reference blank spectrum (bottom); superimposed spectra are from 50 µg/mL solutions of the indicated element in 1% HNO_3. Vertical scale sensitivity is 10 times that of Figure 14.

figure, the accepted relative abundances of the isotopes of Cu, Rb, and Ag were observed. The mass spectrum of Cd is shown in Figure 16; again, the count rates for the various isotopes corresponded to the accepted relative isotopic abundances. Adjacent masses are adequately resolved. The peaks are symmetrical and nearly triangular, as expected for quadrupole mass analysis of ions having a low kinetic energy spread. The least abundant Cd isotope ($^{108}Cd^+$, 0.88%) is clearly detected. For the elements shown in Figures 15 and 16, and for most of the elements studied, only monatomic, singly charged ions were observed. The only cluster ions observed that contained atoms of trace elements were the diatomic oxide, MO^+. Also, no Cu^+ or Mo^+ ions were observed from the orifice assembly, resulting in remarkably simple mass spectra for the trace elements studied.

The utility of the ICP-MS approach for the direct determination of isotopic abundances of elemental constituents in solutions is illustrated further by the data shown in Table V. The agreement with the accepted values of the relative abundances of $^{63}Cu^+$ and $^{65}Cu^+$ is within the estimated uncertainty in the determined values. The absolute standard deviation of the count is approximately 5 times greater than the square root of the average count, which indicates that the uncertainty in the count is significantly greater than the uncertainty expected from counting statistics. This increased uncertainty is undoubtedly due to instability of some

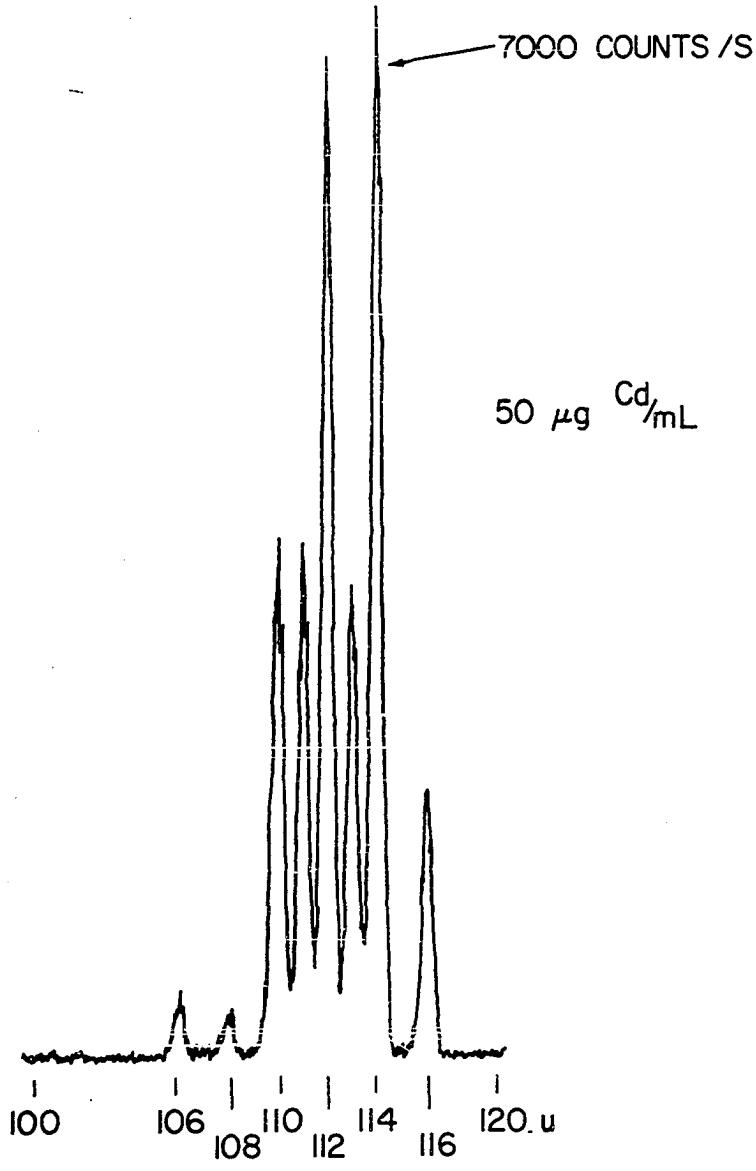

Figure 16. Mass spectrum of Cd in 1% HNO_3. Refer to Table III for isotopic abundances.

instrumental parameter; instability in nebulizer efficiency and ion extraction efficiency through the boundary layer are likely culprits. The precision obtainable for isotopic abundance measurements is expected to improve as these instrumental sources of uncertainty are gradually reduced in future work.

Table V. Relative Isotopic Abundance Determination of Naturally Occurring Copper Isotopes, 2.5 ug/mL Cu in 1% HNO_3.

Isotope	N	σ	$N^{1/2}$	% Abundance Determined	Accepted
$^{63}Cu^+$	19786	740	143	69.9 ± 1.1	69.1
$^{65}Cu^+$	8505	546	98	30.1 ± 1.1	30.9

N = background-subtracted average count, obtained in single ion mode as described in Chapter II. Uncertainties are indicated at 95% confidence level for 15 determinations.

Chromium and copper are clearly detected at the 0.05 ug/mL level in a scanning mode as shown in Figure 17. At this vertical scale sensitivity the minor peaks in the reference blank spectrum were readily observable, but $^{52}Cr^+$, $^{63}Cu^+$, and $^{65}Cu^+$ remained free of interference and were readily detectable at peak heights of 75-150 counts/s above the reference blank level (30 counts/s). In a similar exper-

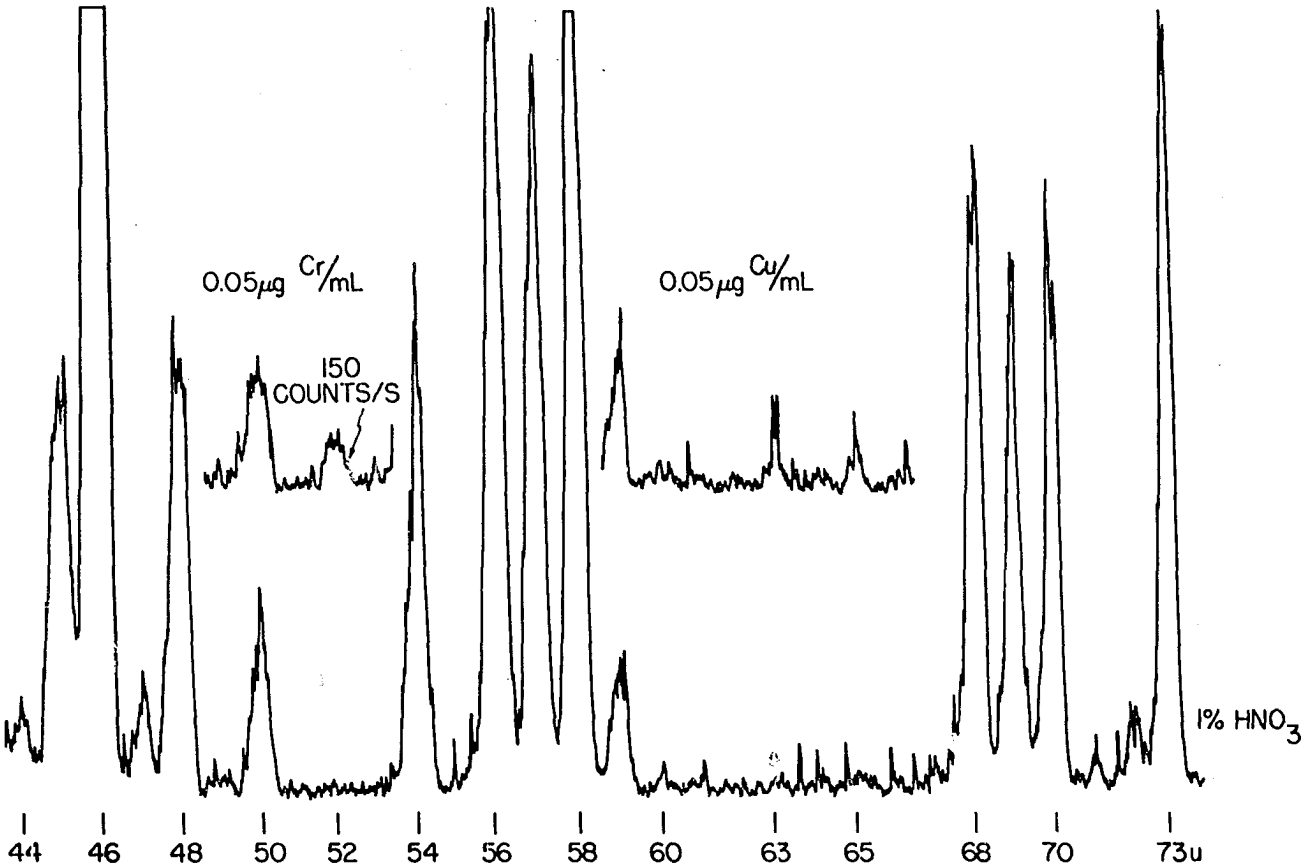

Figure 17. Reference blank spectrum (bottom); superimposed spectra are of indicated solutions in 1% HNO_3. Reference blank count rate at 52, 63, and 65 u was approximately 30 counts/s.

iment, $^{55}Mn^{+}$ at 0.05 ug/mL was clearly detectable in the scanning mode as a peak of approximately 150 counts/s on the low mass edge of the peak at 56 u in the reference blank spectrum. These results show that the ICP-MS technique, even in the scanning mode and at this state of development, is applicable for the detection of elemental and isotopic species at trace and near ultratrace levels. Continued instrumental development and optimization are expected to increase the transmission of trace element ions and reduce the photon and minor ion contributions to the reference blank count rate, leading to further improvement in the powers of detection.

The analytical calibration curves shown in Figure 18 were obtained in the single ion mode with reference solutions that contained only one element. Although significant long-term drift is evident, the curves were linear over nearly four orders of magnitude. Both Co and Mn were easily detected at the 0.02 ug/mL level. In addition, the count rates obtained for identical concentrations of Co and Mn on the same day were similar. These two elements are similar in mass and ionization energy, and both elements yield only singly charged, monatomic ions from the ICP plume. Therefore, these two elements are expected to be extracted from the ICP plume with similar efficiency. The similarity of the count rates for a given concentration of these two elements (along with the major isotope of chromium, $^{52}Cr^{+}$,

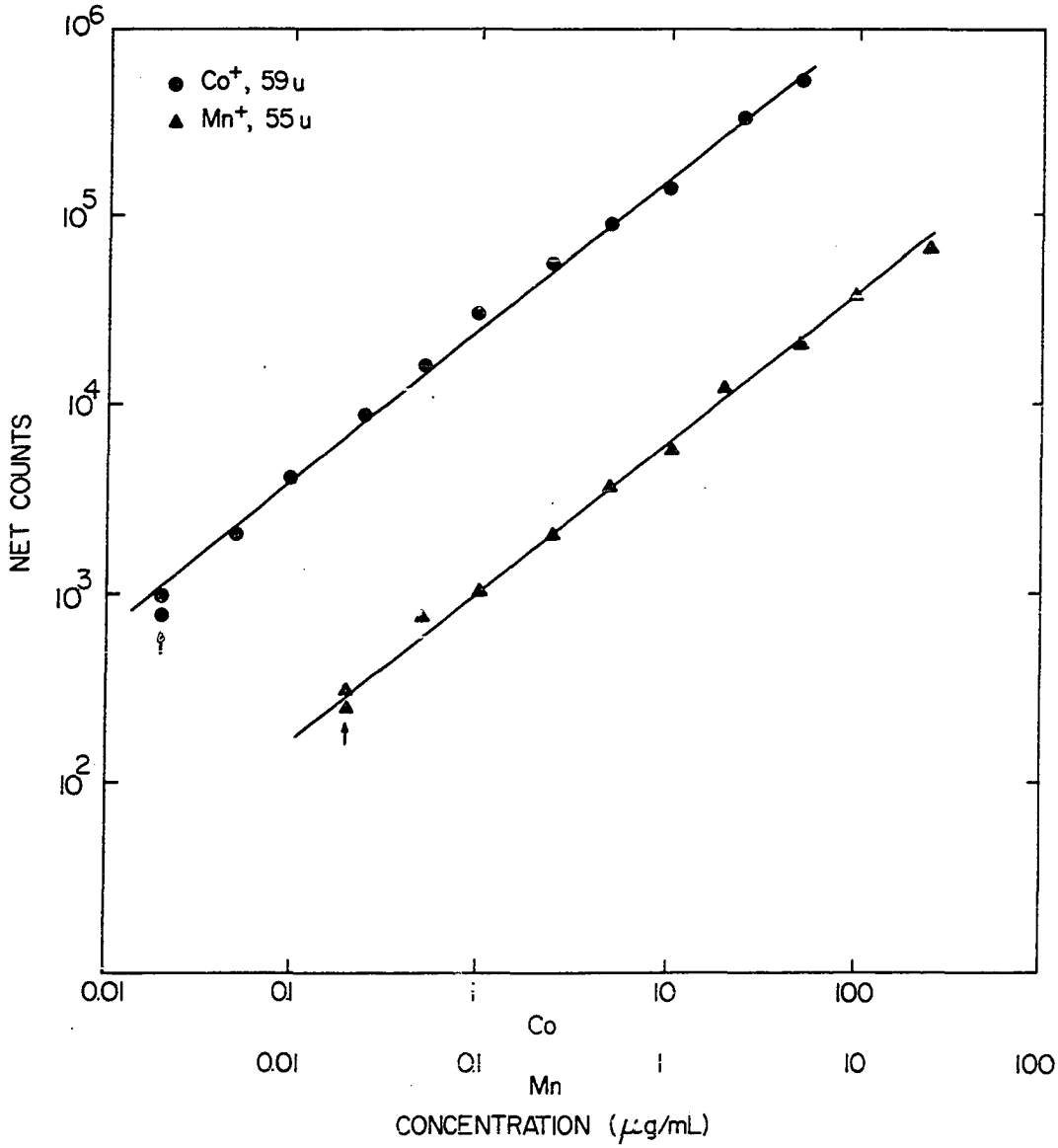

Figure 18. Analytical calibration curves for Co and Mn. Note shift of concentration axis for Mn. Both curves were obtained with the same sampler.

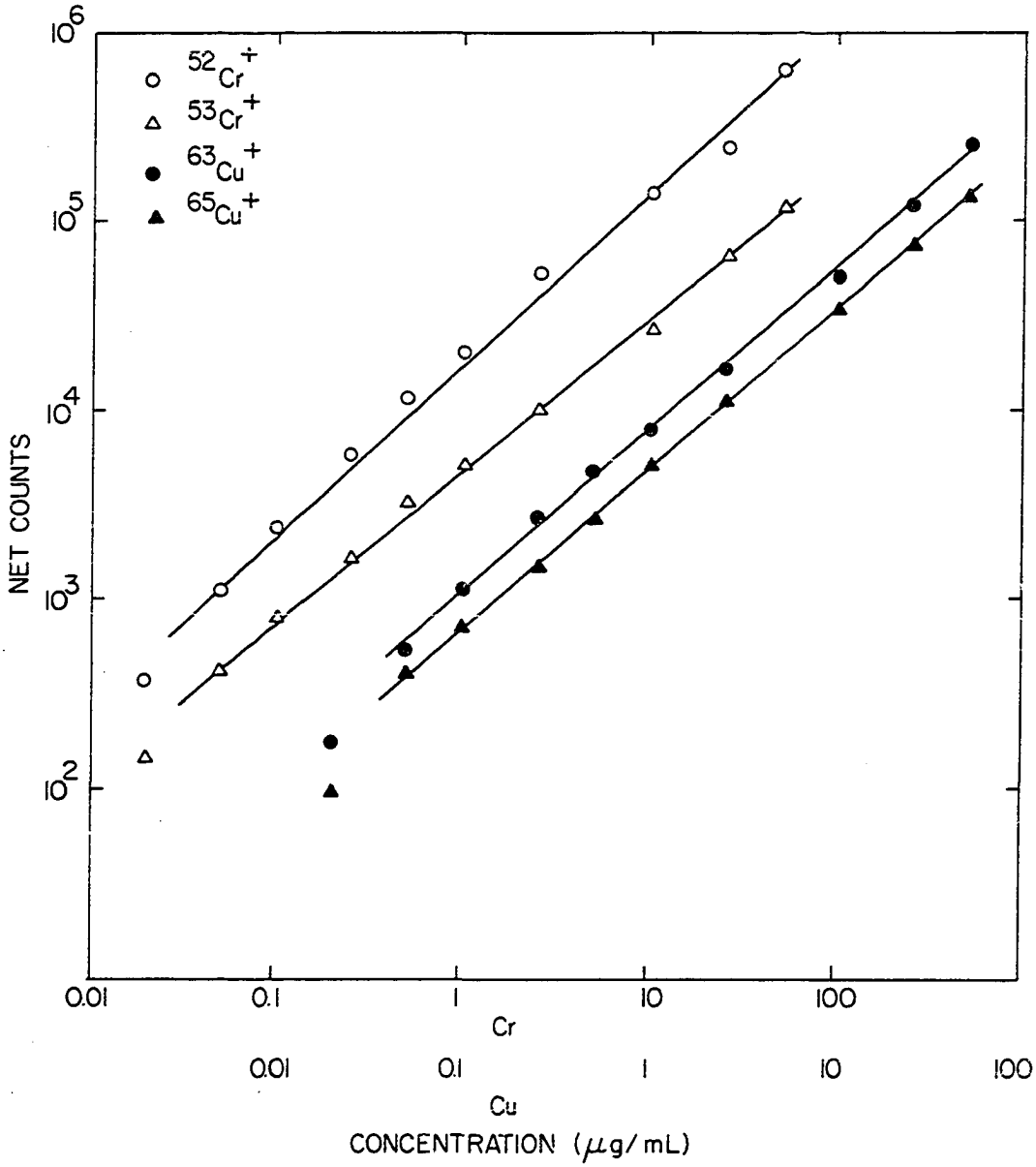

Figure 19. Analytical calibration curves for $^{52}Cr^+$, $^{53}Cr^+$, $^{63}Cu^+$, and $^{65}Cu^+$. Refer to Table III for isotopic abundances. Note shift of concentration axis for Cu.

shown in Figure 19), indicates that it may be possible to combine the elements into groups having similar extraction and transmission efficiencies. This observation suggests the possibility of basing survey-type determinations of a large number of elements on analytical calibration data obtained for only one or two elements in each group.

The curves in Figure 18 show replicate determinations at the 0.02 ug/mL level. For both elements the point labeled with the arrow was determined first, followed by the unlabeled point after the rest of the analytical calibration data were obtained. This small positive deviation reflects the general tendency of the count rates of all the ions to increase slowly with time (10-40% every hour) in the absence of orifice plugging. This gradual increase is not caused by any discernible increase in the orifice diameter. The rate of increase is greatest for the first 15 minutes after the ICP plume is positioned adjacent to the sampler. Ion extraction conditions only approach a steady state after approximately 1 hour.

Analytical calibration curves for the two most abundant Cr isotopes and the two Cu isotopes are shown in Figure 19. The curves for the less abundant isotopes lie consistently below those for the major isotope. The less abundant isotopes of both Cr and Cu are thus useful for analysis. In an application of the ICP-MS approach to multielement analy-

sis, it is anticipated that the ability to use less abundant isotopes may be necessary to avoid spectral interferences from background ions (e.g., $Ar^+ \cdot H_2O$ interfering with $^{58}Ni^+$ (67.88%)) or from other elements present in the samples. Such interferences are especially troublesome when a quadrupole mass analyzer is used, because of its inability to resolve chemically different ions of the same mass number. Especially troublesome interferences might be expected from the less abundant isotopes of major elements, e.g., $^{48}Ca^+$ interfering with $^{48}Ti^+$. In hard water samples with different Ca concentration (perhaps 500 to 600 ug/mL), the background count rate at 48 u would not be correctly evaluated by simple subtraction of the average count at 48 u for a reference blank solution, whose Ca concentration may be significantly different from that of the samples. However, as long as one isotope of each major element can be observed without interference, the contribution of each potentially interfering isotope can be calculated from the accepted isotopic abundance ratios and subtracted from the measured count at the mass of interest. The limited number of potential spectral interferences observed in the ICP mass spectra facilitates such a straightforward correction procedure.

The observed detection limits are listed for selected elements in ug/mL and parts-per-million atomic (ppma) in Table VI. The detection limits for the major isotopes of Cr,

Cu, and Rb are lower than those for the corresponding minor isotopes by factors approximately equal to the relative isotopic abundances. Although the background-subtracted average counts obtained for $^{52}Cr^+$, $^{55}Mn^+$, and $^{59}Co^+$ are nearly identical, the detection limits for these three elements are significantly different. The trend of these values can be readily reconciled by referring to Figure 17, which shows that $^{52}Cr^+$ is free of spectral interference, $^{55}Mn^+$ falls between two peaks in the reference blank spectrum, and the peak due to $^{59}Co^+$ coincides with a peak in the reference blank spectrum. The standard deviation of the reference blank count thus increases in the order 52 u < 55 u < 59 u. The two cases of spectral interference illustrated above are likely to occur in the analysis of real samples with a low resolution quadrupole mass analyzer. Such interferences can be circumvented using less abundant isotopes that are free of interference at the expense of a reduction in the powers of detection. It is clearly desirable to reduce both the number and count rates of minor ions in the reference blank spectrum. Because many of these minor ions are clusters and are probably formed during the ion extraction process, the desired simplification of the reference blank spectrum may be achievable by improving the ion sampling interface.

As shown in Table VI and Figure 20, arsenic was detected as As^+ (75 u) and AsO^+ (91 u). The observed ratio As^+/AsO^+

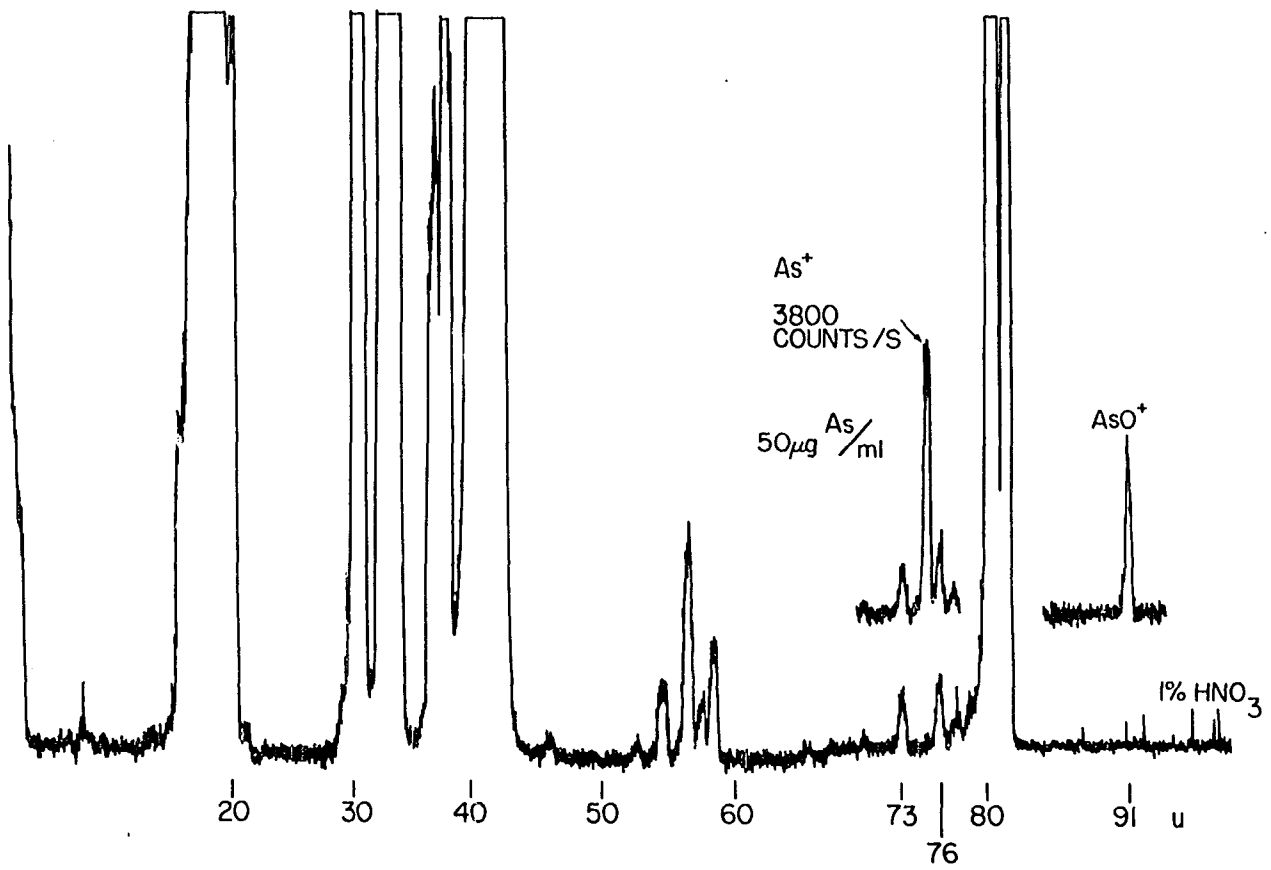

Figure 20. Reference blank mass spectrum (bottom) with mass spectrum for 50 μg/mL As superimposed.

Table VI. Detection Limits Obtained.

ELEMENT	ION(S) DETECTED	%ABUNDANCE	DETECTION LIMIT ug/mL	ppma
Mg	$^{24}Mg^+$	78.6	0.006	0.004
Cr	$^{52}Cr^+$	83.8	0.002	0.0007
	$^{53}Cr^+$	9.6	0.01	0.003
Mn	$^{55}Mn^+$	100	0.003	0.001
Co	$^{59}Co^+$	100	0.006	0.002
Cu	$^{63}Cu^+$	69.1	0.009	0.002
	$^{65}Cu^+$	30.9	0.02	0.005
Rb	$^{85}Rb^+$	72.2	0.008	0.002
	$^{87}Rb^+$	27.8	0.02	0.004
As	$^{75}AsO^+$	100	0.06	0.01
Y	$^{89}YO^+$	100	0.04	0.008

was significantly different for different samplers. Yttrium was also detected as both Y^+ and YO^+. The detection limits listed in Table VI were obtained with a sampler that provided more AsO^+ and YO^+ than As^+ and Y^+, hence the oxide ions were used for the determinations of the detection limits. Although its detection limit was not determined, praeseodymium was detectable only as PrO^+. Apparently, some elements have a high probability of oxide formation. This phenomenon is not expected to cause serious spectral interferences, because a) most of the elements are not detected as oxide ions, and b) the masses and isotopic distribution of MO^+ ions are predictable for those elements with a high probability of oxide formation.

The detection limits and analytical calibration curves reported above were reproducible to within 20% during a

single day's run of 5 to 10 hours, or for as long as an orifice remained unplugged by condensation of solids. The above results were also reproducible to within 50% from day to day for the same sampler. Nearly linear analytical calibration curves were obtained with all the samplers used. The detection limits and count rates for reference solutions of the elements studied were reproducible within a factor of 2 for the several samplers used.

The various ionic species detected for the elements studied to date are shown in Table VII. Most elements yield essentially singly charged, monatomic, positive ions. Strontium and barium gave the only doubly charged analyte ions observed. Both of these elements have low second ionization potentials. The presence of these doubly charged ions is expected to provide serious spectral interference in only a few cases, e.g, $^{130}Ba^{+2}$ with $^{65}Cu^{+}$, and neither element is expected to be present at high levels in most real samples. Thus, the potential spectral interferences from doubly charged analyte ions is not expected to be severe.

Those oxide ions observed are mostly from elements recognized as yielding refractory or strongly-bound oxides in other spectrochemical sources (139). In the case of As and Y, the oxide ions were used for the detection limit determinations. The other oxide ions observed could be readily anticipated; although they sometimes coincide with analyte

masses, e.g., $^{48}TiO^+$ with $^{64}Zn^+$, such spectral interference could be readily anticipated and offers prohibitive interference with only a few elements. The mass spectrum of analyte ions from the ICP is much simpler than that obtained from most ion sources investigated for elemental determinations in solutions (65, 140). Also, the ratio MO^+/M^+ for a given oxide-forming element varies for different samplers and tends to increase with boundary layer thickness, indicating that some control over the degree of MO^+ formation may be possible by optimization of the boundary layer thickness.

As shown in Figure 21, iodine yielded mostly I^+ with a few percent HI^+. Negative ions could not be determined with the present apparatus. Bromine gave a similar spectrum but many less positive ions, while chlorine was not detectable as a positive ion. This trend is expected because the ionization energy and electron affinity of the halogens increase in the order I < Br < Cl. Thus the probability of forming positive ions decreases while the probability of forming negative ions increases in the order I < Br < Cl.

Figure 22 shows nearly identical mass spectra (Br^+ and HBr^+) obtained from approximately equimolar solutions of NaBr and $NaBrO_3$. No oxide ions such as BrO^+ were detected. Iodine mass spectra (I^+, HI^+) obtained from equimolar solutions of NaI and $NaIO_3$ were also nearly identical with no oxide ions. Apparently, the aqueous ions of these elements

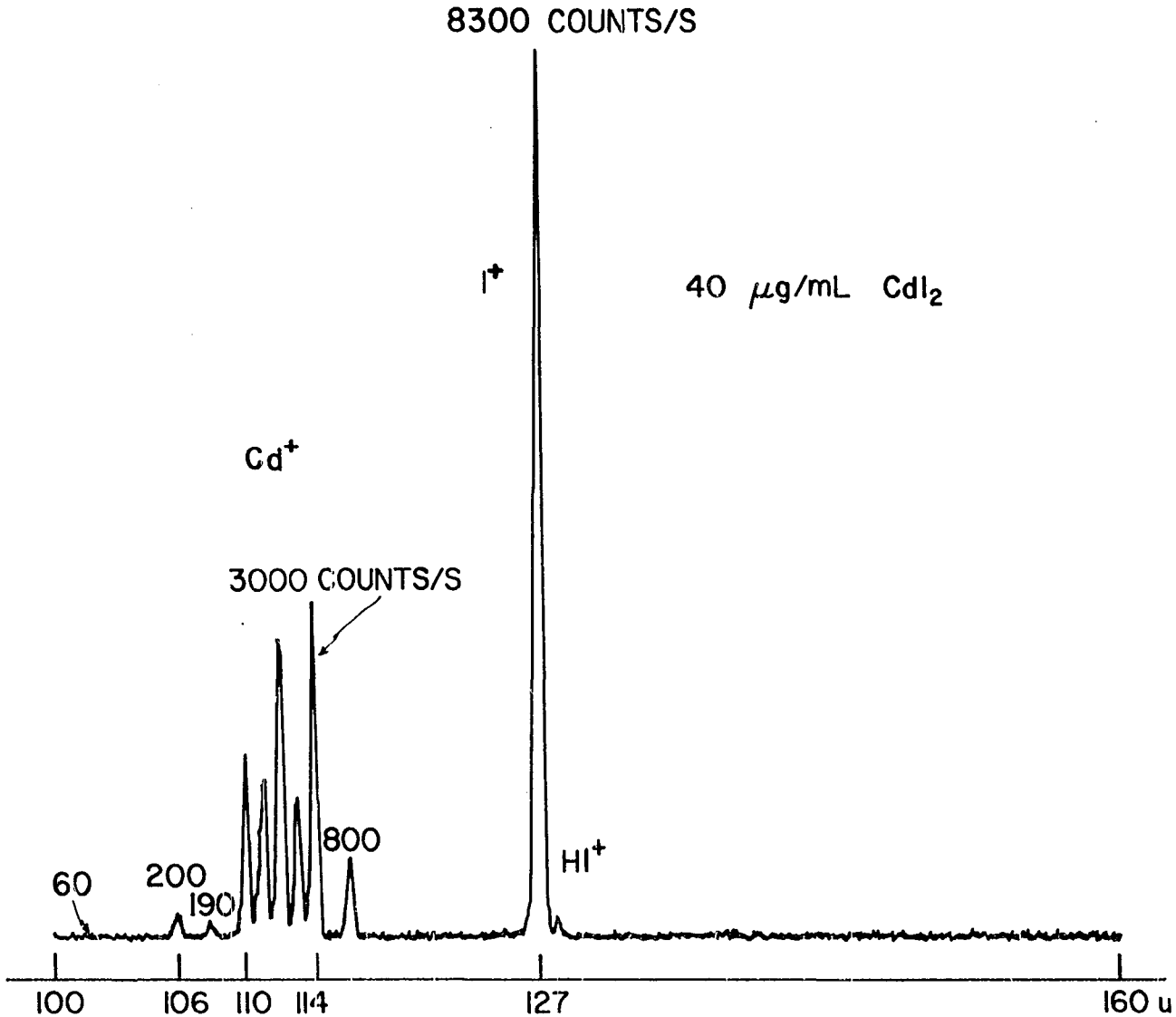

Figure 21. Mass spectrum of CdI_2 solution in 1% HNO_3.

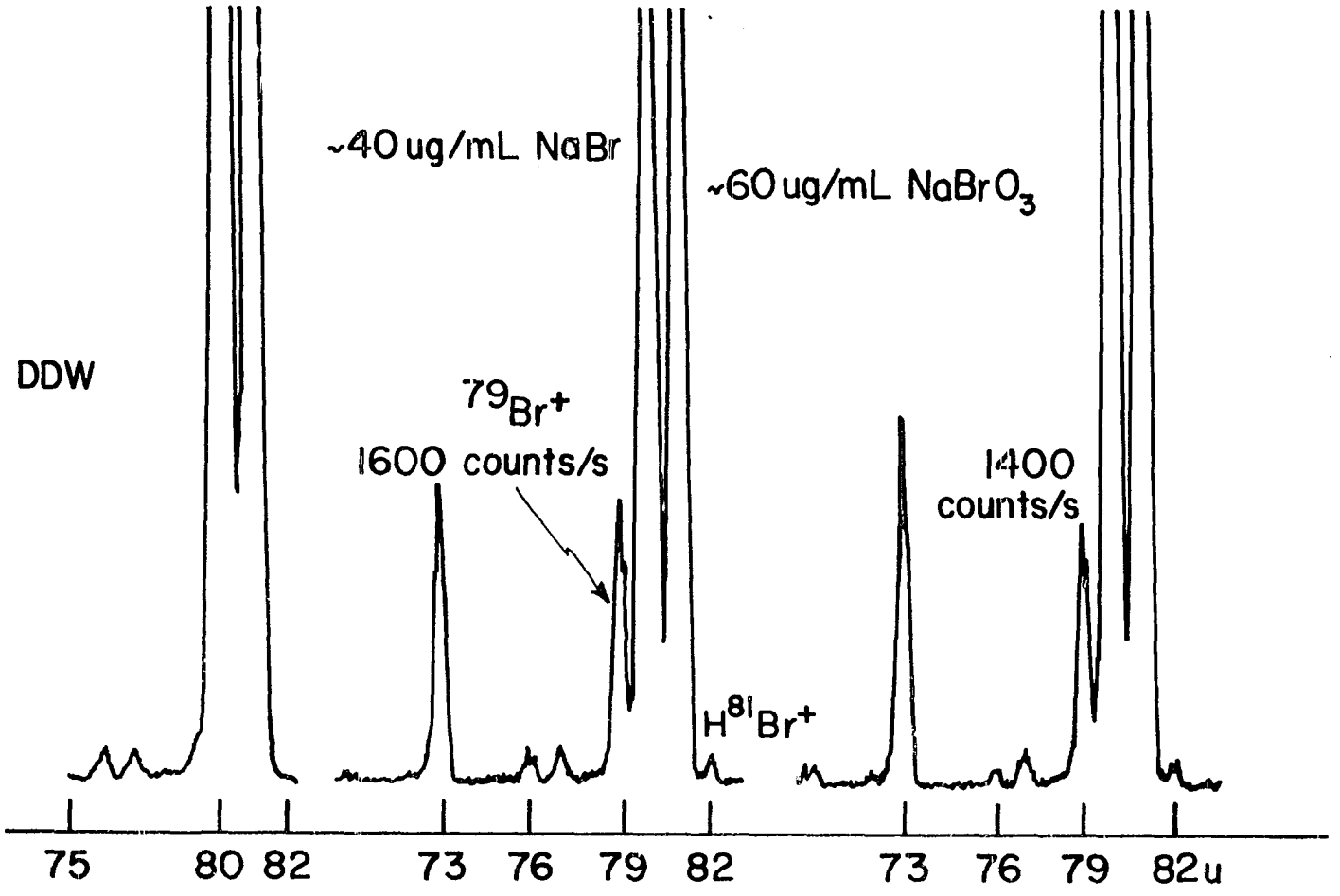

Figure 22. Mass spectra of deionized distilled water (DDW), and approximately equimolar solutions of NaBr and $NaBrO_3$.

Table VII. Ionic Species Detected for Analyte Elements Studied to Date.

ELEMENT	ION	MASSES (u)
Li	Li^+	6,7
Na	Na^+	23
Mg	Mg^+	24,25,26
K	K^+	39
Ti	Ti^+	46-50
	TiO^+	62-66
V	V^+	50,51
Cr	Cr^+	50,52-54
Mn	Mn^+	55
Ni	Ni^+	58,60-62,64
Cu	Cu^+	63,65
Zn	Zn^+	64,66-68,70
As	As^+	75
	AsO^+	91
Br	Br^+	79
	HBr^+	82
Rb	Rb^+	85,87
Sr	Sr^+	84,86-88
	Sr^{+2}	42-44
	$SrOH^+$	103-105
Y	Y^+	89
	YO^+	105
Mo	Mo^+	92,94-98,100
Ag	Ag^+	107,109
Cd	Cd^+	106,108,110-114,116
I	I^+	127
	HI^+	128
Cs	Cs^+	133
Ba	Ba^+	130,132,134-138
	Ba^{+2}	65,66,67-69
	BaO^+	146,148,150-154
Pr	PrO^+	157
Hg	Hg^+	196,198-202,204
Pb	Pb^+	204,206-208

are completely atomized in the ICP. Incomplete atomization of $NaBrO_3$ would limit the number density of free Br atoms, thus suppressing the formation of Br^+ from $NaBrO_3$ relative to

NaBr. Various reviews characterize the ICP as being efficient at dissociating compounds into free atoms; the equality of the Br^+ signals from similar atomic concentrations of NaBr and $NaBrO_3$ supports this conclusion.

Stripchart recordings of the count rate in the single ion mode as a function of time are shown in Figure 23. Aerosol of a new solution first reaches the ICP about 1 minute after the change of solution. Once the analyte aerosol reaches the ICP, the ion count rate of the mass of interest rises rapidly to a constant value. For the bottom two tracings in Figure 23, which were obtained with the nebulizer producing an exceptionally intense and stable mist, the noise at the top of the peak is nearly equal to the expected shot noise of the electron multiplier, i.e., $\sigma = N^{\frac{1}{2}}$. In the top tracing the nebulizer was producing a visibly unsteady mist, resulting in an ion count rate which fluctuated between various values. Regardless of the state of the transducer and mist produced, the ion counts decreased rapidly as the particular analyte was rinsed from the nebulizer, i.e., the 1% level was obtained approximately 15 s after the rinse solution reached the transducer surface. These "rinse-out" profiles are nearly the same as those obtained by ICP-AES using this ultrasonic nebulizer, indicating that the presence of the ion sampling interface introduced little or no memory. Certainly, there was no evidence of

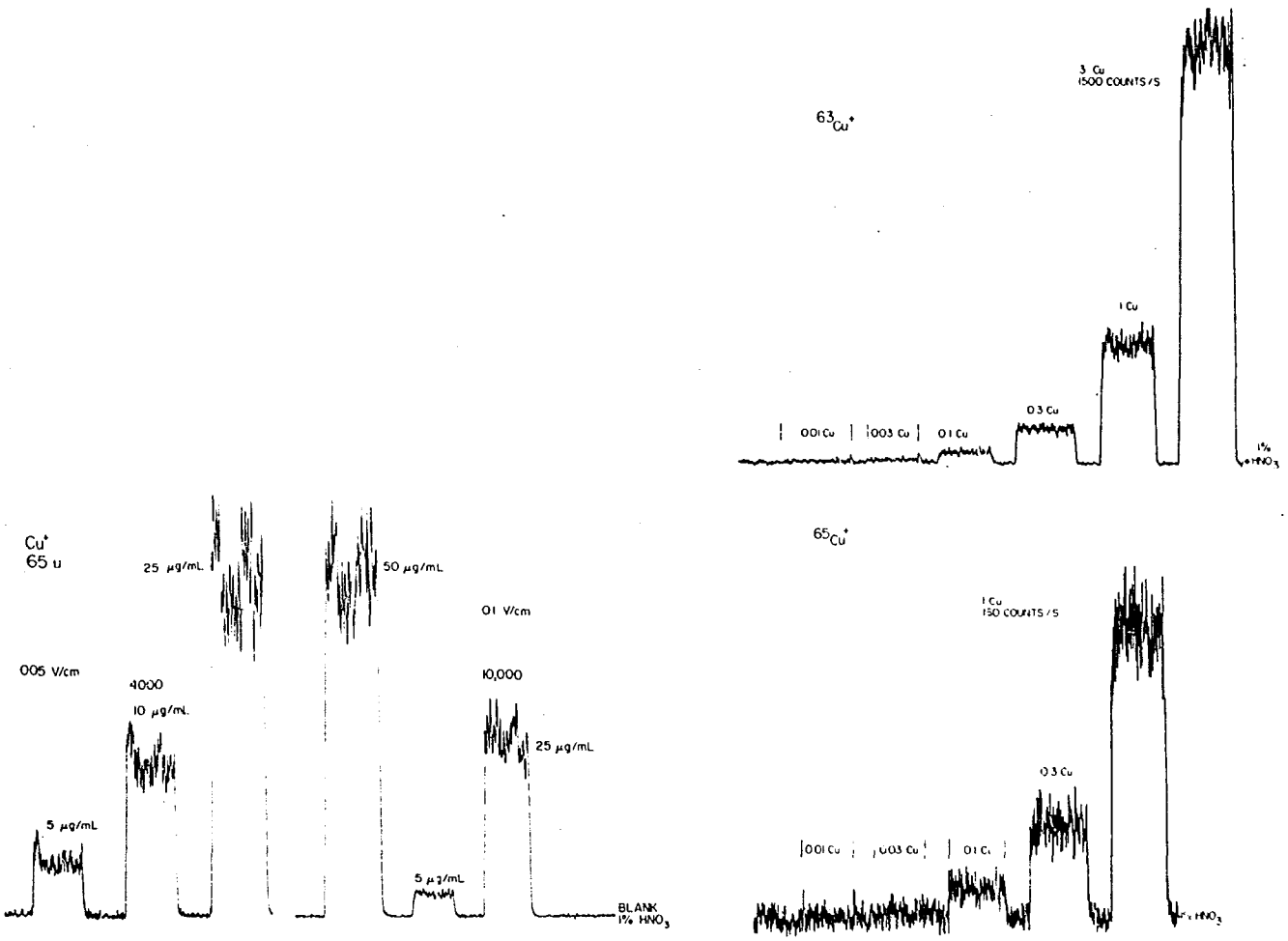

Figure 23. Analyte ion count rate (vertical axis) as a function of time (horizontal axis) in single ion mode at indicated mass. Baseline corresponds to count rate for blank solution. One inch on horizontal axis corresponds to approximately 10 minutes.

memory between reference solutions if the nebulizer was rinsed between experiments with the reference blank solution unless a large amount of solid was deposited upon the skimmer and sampler cones.

As mentioned above, the ICP as a VAEI cell for optical emission spectrometry is relatively free from ionization interferences caused by easily ionized concomitant elements in solution. For example, the intensities of certain emission lines of excited ions of Ca, Cr, and Cd show little dependence on Na concentrations from 0 to 7000 ug/mL (86). In the present work, the count rates of analyte ions were suppressed to a somewhat greater extent in the presence of Na. Figure 24 shows plots for Cr^+ and Co^+ (10 ug/mL solution concentration) as a function of Na concentration. Each point is normalized to a reference count rate for the same solution concentration of the analyte ion in the absence of Na. Because Na concentrations $\geq$ 100 ug/mL gradually clog the orifice with condensed solid, the reference count rate gradually decreases and is therefore determined repeatedly. The arbitrary nature of this correction procedure, coupled with a significant long-term drift in the intensity of the mist produced by the ultrasonic transducer (e.g., left plot in Figure 23), led to the scatter of the points shown in Figure 24. These plots have a shape similar to that observed for optical emission spectrometry by Larson et al. (86). Because an ultrasonic

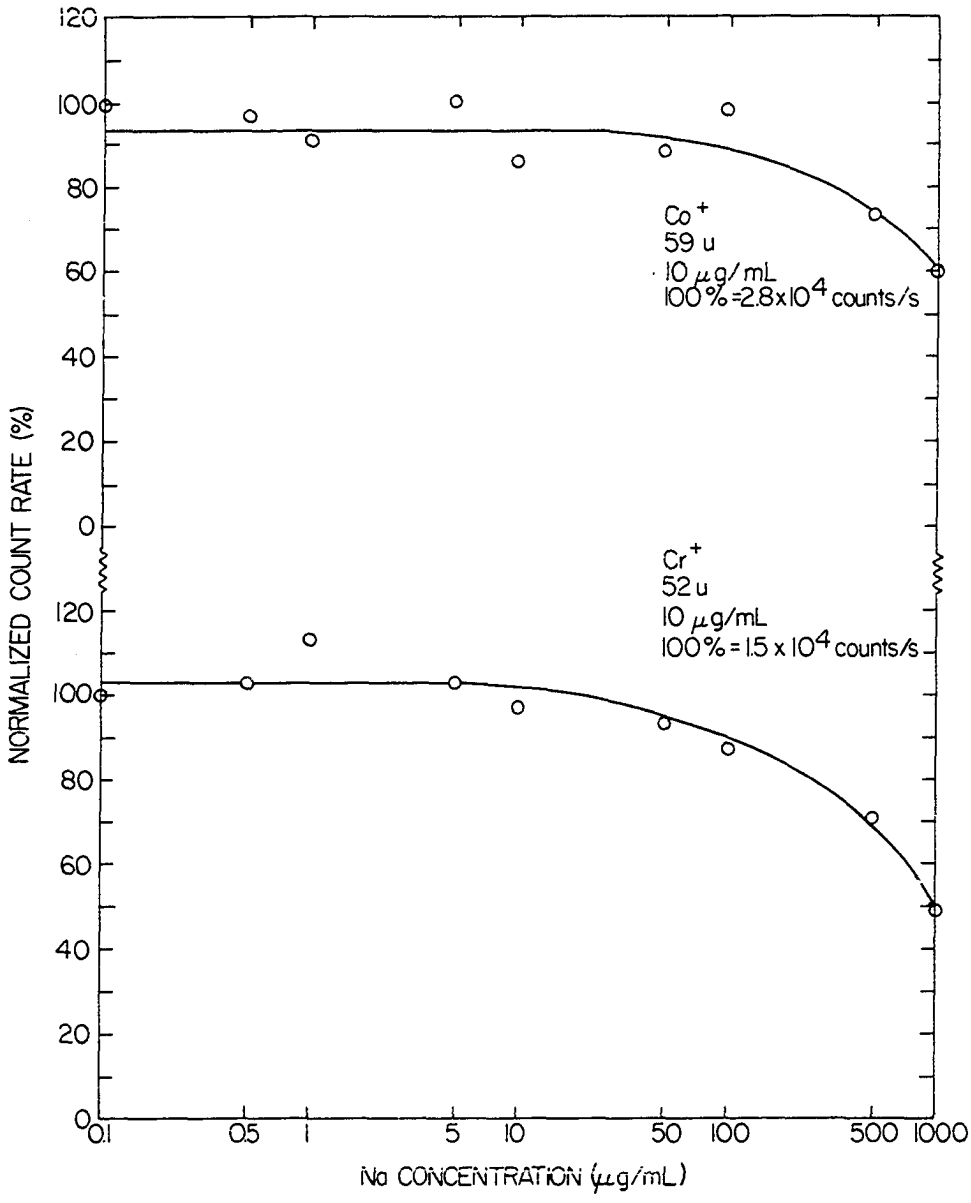

Figure 24. Effect of Na concentration on count rates of $^{52}Cr^{+}$ and $^{59}Co^{+}$, single ion mode, 10 s count time, approximately 5 count periods averaged.

nebulizer was used in the present work, 1000 ug/mL Na corresponds roughly to 10,000 ug/mL Na in Larson's work, which was performed with a pneumatic nebulizer.

The larger magnitude of suppression of analyte ionization observed in the present work (compared to similar studies done by atomic emission spectrometry) may be rationalized as follows. In the present work, ion extraction occurrs through an unbroken boundary layer that is somewhat cooler than the unperturbed plasma. Ion-electron recombination or electron loss to the sampler wall may occur at a significant rate in this layer, leading to an effective n_e in the vicinity of the orifice that is less than that prevalent in the unperturbed plasma. For this lower value of n_e, the "extra" electrons contributed by the ionization of Na should be more significant, causing a proportionately greater increase in the total n_e near the orifice. Thus, the greater suppression of analyte ionization observed in the present work may be a characteristic of the boundary layer rather than the unperturbed plasma. A strict comparison of the magnitudes of the ionization suppressions observed in the present work and those observed by atomic emission spectrometry is not necessarily valid.

These results indicate that reference standard and sample solutions need to be closely matched with regard to the concentrations of easily ionized concomitants at levels

above 100 ug/mL. Orifice plugging is a more serious problem. Normalization of analyte ion count rates to either an internal standard ion or a beam monitor could correct for the decrease in extraction efficiency of ions due to moderate solid condensation. However, the plugging problem severely restricts the time that an orifice can be exposed to solutions whose total solute concentration is above approximately 100 ug/mL. Although the elevated temperature of the sampler inhibits the condensation of solids at the orifice, this orifice plugging problem must be alleviated further before the ICP-MS technique can become useful for the determination of trace elements in many real samples.

CHAPTER IV. SUMMARY AND OBJECTIVES FOR FUTURE RESEARCH

The basic objectives of this feasibility study have been demonstrated. The elemental and isotopic composition of reference solutions can be determined directly by ICP-MS in its present state of development with negligible sample pretreatment. A realistic sample throughput rate of one every 5 minutes (largely determined by the nebulizer cleanout time) is possible. Positive ion mass spectra from the ICP are simple with relatively few spectral interferences. Most analytes are detected as M^+ ions in the accepted relative isotopic abundances. Some analytes such as As and Y yield both M^+ and MO^+ ions. The simple, uncluttered nature of both the background and analyte mass spectra, along with the low kinetic energy spread of the ions, makes possible the use of a quadrupole mass analyzer of modest resolution. The powers of detection are already sufficient for elemental and isotopic determinations near ultratrace levels with a linear dynamic range of at least four orders of magnitude.

The first objective for future research is the improvement of the analytical performance of the ICP-MS approach. Therefore, further development of this technique will focus on several practical problems. The orifice assembly described in the present work needs to be improved. An orifice of diameter > 50 um would plug less easily while extracting

more ions into the vacuum system. The expected advantages make the effort to construct orifice assemblies that can withstand the "pinch effect" worthwhile. Further improvements in the vacuum system, ion lens, mass spectrometer, and detector are also expected to increase the transmission of analyte ions and decrease the background levels (minor ions + photons). These experiments will concentrate successively on optimization of each of the physical processes fundamental to the technique. The performance of the ICP-MS technique with regard to analytical figures of merit should improve as a result of these refinements.

The second objective for future research is the application of the ICP-MS approach to real analytical problems. This objective will involve a) evaluation of accuracy and precision by analysis of standard samples, b) evaluation of possible interferences in the analysis of real samples, i.e., ionization interferences, mass spectral interferences, and orifice plugging, and c) interfacing the ICP-MS instrument to a digital computer for rapid mass programming and data acquisition.

The real value of the ICP-MS approach will lie in its eventual contribution to the solution of real analytical problems. The above figures of merit indicate that the ICP-MS technique is potentially competitive with most currently accepted methods for multielement analysis of solutions, and

more than competitive if the determination of isotopic distributions for a large number of solutions is desired. Because of the versatile data acquisition capabilities of the quadrupole mass analyzer, this technique is potentially capable of a) survey or semiquantitative determinations of nearly all the elements, or b) rapid quantitative determinations of a selected group of elements. Both of these capabilities are not generally found in existing instrumentation suitable for multielement analysis of solutions. The present work describes the courtship and the wedding ceremony of the best features of inductively coupled plasmas and mass spectrometry, which are two of the most powerful fields of instrumental analysis. Energetic development should produce a long and fruitful marriage between these two techniques.

LITERATURE CITED

1. Dulka, J. J.; Risby, T. H. Anal. Chem. 1976, 48, 640A-653A.

2. Goyer, H. A.; Mehlman, M. A., Eds. "Toxicology of Trace Elements"; Hemisphere: Washington, 1977; Vol. 2.

3. Morgan, G. B.; Bretthauer, E. W. Anal. Chem. 1977, 49, 1210A-1214A.

4. Schroeder, H. A. "The Poisons Around Us", Indiana University: Bloomington, 1974.

5. Schroeder, H. A. In "Environmental Problems in Medicine"; McKee, W. D., Ed.; Charles C. Thomas: Springfield, Illinois, 1974; Chapters 23 and 24.

6. Underwood, E. J. "Trace Elements in Human and Animal Nutrition", Academic: New York, 1977.

7. Environmental Studies Board, National Academies of Science and Engineering, "Water Quality Criteria 1972". EPA-R3-73-033, 1973.

8. Environmental Protection Agency (U. S.) "Quality Criteria for Water". Government Printing: Washington, D. C., 1976; Fed. Register March 15, 1979, 44, 15926-15981.

9. Salin, E. D.; Ingle, J. D., Jr. Anal. Chem. 1978, 50, 1737-1744, 1745-1752.

10. Lundberg, E.; Johansson, G. Anal. Chem. 1976, 48, 1922-1926.

11. Macdonald, G. L. Anal. Chem. 1978, 50, 135R-142R.

12. Johansson, S. A. E.; Johansson, T. B. Nucl. Instrum. Methods 1976, 137, 473-516.

13. Clark, P. J.; Neal, G. T.; Allen, R. O. Anal. Chem. 1975, 47, 650-658.

14. Op de Beeck, J.; Hoste, J. Analyst (Lond.) 1974, 99, 973-993.

15. DeSoete, D.; Gijbels, R.; Hoste, J. "Neutron Activation Analysis"; Wiley-Interscience: London, 1972; Chapter 1.

16. Berry, P. T.; Martin, T. C. In "Advances in Activation Analysis", Lenihan, J. M. A.; Thomson, S. J.; Guinn, V. P., Eds.; Academic: New York, 1972; Vol. 2.

17. Deconninck, G. Nucl. Instrum. Methods 1977, 142, 275-284.

18. Vydra, T.; Stulik, K.; Julakava, E. "Electrochemical Stripping Analysis"; Tyson, J., translation Ed.; Ellis Harwood: Chichester, England, 1976.

19. Drawin, H. W. In "Plasma Diagnostics", Lochte-Holtgreven, W., Ed.; Wiley: New York, 1968; Chapter 13.

20. Fehsenfeld, F. C.; Schmeltekopf, A. L.; Ferguson, E. E. J. Chem. Phys. 1966, 44, 4087-4094, 4095-4103; J. Chem. Phys. 1967, 46, 2802-2808.

21. Fite, W. L. Int. J. Mass Spectrom. Ion Phys. 1975, 16, 109-124.

22. Siegel, M. W.; Fite, W. L. J. Phys. Chem. 1976, 80, 2871-2881.

23. Studniarz, S. A.; Franklin, J. L. J. Chem. Phys. 1968, 49, 2652-2659.

24. Franklin, J. L.; Studniarz, S. A.; Ghosh, P. K. J. Chem. Phys. 1968 39, 2050-2061.

25. Fristrom, R. M.; Westenburg, A. A. "Flame Structure", McGraw-Hill: New York, 1965, Chapter 9.

26. Fristrom, R. M. Int. J. Mass Spectrom. Ion Phys. 1975, 16, 15-32.

27. Goodings, J. M.; Bohme, D. K.; Ng, C. W. Combust. Flame 1979, 36, 27-43.

28. Hasted, J. B. Adv. Mass Spectrom. 1974, 6, 901-914.

29. Hasted, J. B. Int. J. Mass Spectrom. Ion Phys. 1975, 16, 3-14.

30. Hastie, J. W. Int. J. Mass Spectrom. Ion Phys. 1975, 16, 89-100.

31. Hayhurst, A. N.; Sugden, T. M. Proc. Roy. Soc. (Lond.) 1966, A293, 36-50.

32. Hayhurst, A. N.; Telford, N. R. Proc. Roy. Soc. (Lond.) 1971, A322, 483-507.

33. Hayhurst, A. N.; Mitchell, F. R. G.; Telford, N. R. Int J. Mass Spectrom. Ion Phys. 1971, 7, 177-187.

34. Hayhurst, A. N.; Telford, N. R. Combust. Flame 1977, 28, 67-80.

35. Hayhurst, A. N.; Kittelson, D. B.; Telford, N. R. Combust. Flame 1977, 28, 123-135, 137-143.

36. Burdett, N. A.; Hayhurst, A. N. Chem. Phys. Lett. 1977, 48, 95-99; Combust. Flame 1979, 34, 119-134.

37. Knewstubb, P. F.; Sugden, T. M. Proc. Roy. Soc. (Lond.) 1960, A255, 520-537.

38. Knewstubb, P. F. "Mass Spectrometry and Ion-Molecule Reactions"; Cambridge University: London, 1969; Chapter 2.3.

39. Greene, F. T.; Brewer, J.; Milne, T. A. J. Chem. Phys. 1964, 40, 1488-1495.

40. Milne, T. A.; Greene, F. T. J. Chem. Phys. 1966, 44, 2444-2449.

41. Milne, T. A.; Greene, F. T. In "Mass Spectrometry in Inorganic Chemistry", Advances in Chemistry Series, Gould, H. F., Ed.; American Chemical Society: Washington, D. C., 1968; Vol. 72, Chapter 5.

42. Milne, T. A.; Beachey, J. R. "Direct Sampling and Characterization of Gaseous Species Responsible for Fireside Corrosion in Fossil Fuel-Fired Systems". Quarterly Progress Reports, ERDA-FE-228-4, 1976-1977.

43. Morley, C. Vacuum 1974, 24, 581-584.

44. Pertel, R. Int. J. Mass Spectrom. Ion Phys. 1975, 16, 39-52.

45. Serauskas, R. V.; Brown, G. R.; Pertel, R. Int J. Mass Spectrom. Ion Phys. 1975, 16, 69-87.

46. Price, D.; Lippiatt, J. H.; Brown, R. W.; Izod, D. C. A. Adv. Mass Spectrom. 1974, 6, 551-555; Int. J. Mass Spectrom. Ion Phys. 1975, 16, 101-108.

47. Prokopenko, S. M. J.; Laframboise, J. G.; Goodings, J. M. J. Phys. D 1972, 5, 2152-2160; J. Phys. D. 1974, 7, 355-362, 563-568; J. Phys. D 1975, 8, 135-140.

48. Rowe, B. Int. J. Mass Spectrom. Ion Phys. 1975, 16, 209-223.

49. Gaucherel, P.; Rowe, B. Int. J. Mass Spectrom. Ion Phys. 1977, 23, 227-235.

50. Segun, J. G.; Dugan, C. H.; Goodings, J. M. Int. J. Mass Spectrom. Ion Phys. 1972, 9, 203-213.

51. Shahin, M. M. J. Chem. Phys. 1966, 45, 2600-2605.

52. Theuws, P. G. A.; Beyerinck, H. C. W.; Schram, D. C.; Verster, N. F. J. Appl. Phys. 1977, 48, 2261-2269.

53. Vasile, M. J.; Smolinsky, G. Int. J. Mass Spectrom. Ion Phys. 1973, 12, 133-146; Int. J. Mass Spectrom. Ion Phys. 1975, 18, 179-192; Int. J. Mass Spectrom. Ion Phys. 1976, 21, 263-277.

54. Braithwaite, A.; Wilson, C. In "Dynamic Mass Spectrometry", Price, D.; Todd, J. F. J., Eds.; Heyden: London, 1978; Vol. 5, Chapter 10.

55. Horning, E. C.; Horning, M. G.; Carroll, D. L.; Dzidic, J.; Stillwell, R. N. Anal. Chem. 1973, 45, 936-943; Anal. Chem. 1975, 47, 1308-1312, 2369-2373; Anal. Chem. 1976, 48, 1763-1768; J. Chromatogr. 1974, 99, 13-21.

56. Karasek, F. N. Industrial Research/Development December 1978, 29, 86-90.

57. Reid, N. M.; French, J. B.; Buckley, J. A.; Lane, D. A.; Lovett, A. M. 25'th Annual Conference on Mass Spectrometry and Allied Topics, Washington, D. C., 1977; Paper No. FP8.

58. Reid. N. M.; French, J. B.; Buckley, J. A.; Lane, D. A.; Lovett, A. M.; Rosenblatt, G. 4'th Joint Conference on Sensing of Environmental Pollutants, 1978; American Chemical Society: Washington, D. C.; Paper No. 158A.

59. Reynolds, W. D.; Mitchum, R. K.; Newton, J.; Bystroff, R. I.; Pomernacki, C.; Brand, H. A.; Siegel, M. W. Chem. Instrum. 1977, 8, 63-98.

60. Siegel, M. W.; McKeown, M. J. Chromatogr. 1976, 22, 397-413; Amer. Lab. November 1975, 10, 89-93.

61. Siegel, M. W.; Fite, W. L. J. Phys. Chem. 1976, 80, 2871-2881.

62. Tsuchiya, M.; Taira, T., submitted for publication in Int. J. Mass Spectrom. Ion Phys., April 1979.

63. Coburn, J. W.; Taglauer, E.; Kay, E. J. Appl. Phys. 1974, 45, 1779-1786; J. Vac. Sci. Technol. 1971, 8, 738-743; Appl. Phys. Lett. 1971, 19, 350-352; Rev. Sci. Instrum. 1970, 41, 1219-1223.

64. Harrison, W. W.; Magee, C. W. Anal. Chem. 1974, 46, 461-464.

65. Bruhn, C. G.; Bentz, B. J.; Harrison, W. W. Anal. Chem. 1979, 51, 673-678, 1853-1855; Int. J. Mass Spectrom. Ion Phys. 1978, 28, 409-425.

66. Colby, B. N.; Evans, C. A., Jr. Anal. Chem. 1974, 46, 1236-1242.

67. Wallace, J. R.; Natusch, D. F. S.; Colby, B. N.; Evans, C. A., Jr. Anal. Chem. 1976, 48, 118-120.

68. Jones, J. L.; Dahlquist, R. L.; Hoyt, R. E. Appl. Spectrosc. 1971, 25, 628-635.

69. Gray, A. L. Proc. Soc. Anal. Chem. 1974, 11, 182-183 ; Anal. Chem. 1975, 47, 600-601; Analyst (Lond.) 1975, 100, 289-299.

70. Gray, A. L. In "Dynamic Mass Spectrometry" Price, D.; Todd, J. F. J., Eds.; Heyden: London, 1975, Vol. 4, Chapter 10.

71. Anderson, F. J.; Gray, A. L. Proc. Anal. Div. Chem. Soc. 1976, 13, 284-287.

72. Gray, A. L. In "Dynamic Mass Spectrometry", Price, D.; Todd, J. F. J., Eds.; Heyden: London, 1975; Vol. 5, Chapter 8.

73. Applied Research Laboratories, Ltd. British Patent 1261596, 1969; U. S. Patent 3944826, 1976.

74. Greenfield, S.; Jones, I. L.; Berry, C. T. Analyst (Lond.) 1964, 89, 713-720.

75. Wendt, R. H.; Fassel, V. A. Anal. Chem. 1965, 37, 920-922.

76. Fassel, V. A. Science 1978, 202, 183-191; Anal. Chem. 1979, 51, 1290A-1308A; Pure Appl. Chem. 1977, 49, 1533-1545.

77. Barnes, R. M. CRC Critical Reviews Anal. Chem. 1978, 7, 203-296.

78. Kalnicky, D. J.; Kniseley, R. N.; Fassel, V. A. Spectrochim. Acta 1975, 30B, 511-525.

79. Kalnicky, D. J.; Fassel, V. A.; Kniseley, R. N. Appl. Spectrosc. 1977, 31, 137-150.

80. Mermet, J. Spectrochim. Acta 1975, 30B, 383-396; C. R. Acad. Sci. (Paris) 1975, 282B, 273.

81. Kornblum, G. R.; de Galan, L. Spectrochim. Acta 1977, 32B, 71-96.

82. Mermet, J. M.; Traissy, C. Rev. Phys. Appl. 1977, 12, 1219-1222.

83. Jarosz, J.; Mermet, J. M.; Robin, J. R. Spectrochim. Acta 1978, 33B, 55-78.

84. Boumans, P. W. J. M.; de Boer, F. J. Spectrochim. Acta 1977, 32B, 365-395.

85. Robin, J. Analusis 1978, 6, 89-97; ICP Inform. Newsletter 1979, 4, 495-509.

86. Larson, G. F.; Fassel, V. A.; Scott, R. H.; Kniseley, R. N. Anal. Chem. 1975, 47, 238-243.

87. Larson, G. F.; Fassel, V. A. Anal. Chem. 1976, 48, 1161-1166.

88. Fassel, V. A.; Kniseley, R. N. Anal. Chem. 1974, 46, 1110A-1120A, 1155A-1164A.

89. Olson, K. W.; Haas, W. J., Jr.; Fassel, V. A. Anal. Chem. 1977, 49, 632-327.

90. Veillon, C.; Margoshes, M. Spectrochim. Acta 1968, 23B, 553-555.

91. Babat, G. I. Vestn. Elektroprom. 1942, 2, 1-12; Vestn. Elektroprom. 1942, 3, 2-8; J. Inst. Electr. Eng. 1947, 94, 27-37.

92. Reed, T. B. Int. Sci. Technol. 1962, 6, 42; J. Appl. Phys. 1961, 32, 821-824, 2534-2535.

93. Floyd, M. A.; Fassel, V. A.; Winge, R. K.; Katzenberger, J. M.; D'Silva, A. P. submitted for publication in Anal. Chem., November 1979.

94. Scott, R. H.; Fassel, V. A.; Kniseley, R. N.; Nixon, D. E. Anal. Chem. 1974, 46, 75-80.

95. Dickinson, G. W. Ph. D. Dissertation, Iowa State University, Ames, IA, 1969.

96. Boumans, P. W. J. M. "Theory of Spectrochemical Excitation"; Hilger and Watts: London, 1966; Chapter 7.

97. Drawin, H. W. Pure Appl. Chem. 1976, 48, 133-153.

98. Kalnicky, D. J. Ph. D. Dissertation, Iowa State University, Ames, IA, 1976.

99. de Galan, L.; Smith, R.; Winefordner, J. D. Spectrochim. Acta 1968, 23B, 521-525.

100. Reed, T. B. J. Appl. Phys. 1963, 34, 2266-2269.

101. Biordi, J. C.; Lazzara, C. P.; Papp, J. F. Combust. Flame 1974, 23, 73-82.

102. Swift, J. D.; Schwar, M. J. R. "Electrical Probes for Plasma Diagnostics"; Elsevier: London, 1969.

103. Peterson, C. A. Ph. D. Dissertation, Iowa State University, Ames, IA, 1977.

104. "CRC Handbook of Chemistry and Physics", 52'nd ed; Chemical Rubber: Cleveland, Ohio, 1972; p. F-35.

105. Castellan, G. W. "Physical Chemistry", 2'nd ed.; Addison-Wesley: Reading, Massachusetts, 1971; Chapter 29.

106. Huheey, J. E. "Inorganic Chemistry"; Harper and Row: New York, 1972; p. 184.

107. Boyd, R. L. F. Proc. Phys. Soc. (Lond.) 1951, 64B, 795-804.

108. Oliver, B. M.; Clements, R. M. J. Phys. D 1975, 8, 914-921.

109. Noor, A. I.; Smy, P. R.; Clements, R. M. J. Phys. D 1977, 10, 1643-1651.

110. Clements, R. M.; Smy, P. R. Combust. Flame 1977, 29, 33-41.

111. Smy, P. R. Adv. Phys. 1976, 25, 517-553.

112. Moak, C. D.; Banta, H. E.; Thurston, J. N.; Johnson, J. W.; King, R. F. Rev. Sci. Instrum. 1959, 30, 694-699.

113. Kistemaker, J.; Rol, P. K.; Politiek, J. Nucl. Instrum. Meth. 1965, 38, 1-11.

114. Giannini, G. M. Sci. Am. August 1957, 197, 80-88.

115. Greenfield, S.; McGeachin, H. McD.; Smith, P. B. Talanta 1975, 22, 1-15.

116. Svec, H. J., lecture notes, Department of Chemistry, Iowa State University, Ames, IA, 1975.

117. Dushman, S. "Scientific Foundations of Vacuum Technique", 2'nd ed.; Lafferty, J. M., Ed.; Wiley: New York, 1962; Chapter 2.

118. Bonjour, P. Rev. Phys. Appl. 1979, 14, 533-540, 715-728.

119. Grivet, P. "Electron Optics"; Pergamon: London, 1965.

120. Harting, E.; Read, F. H. "Electrostatic Lenses"; Elsevier: Amsterdam, 1976.

121. Klemperer, O.; Barnett, M. E. "Electron Optics", 3'rd ed.; Cambridge University: London, 1939.

122. Mulvey, T.; Wallington, M. J. Repts. on Prog. Phys. 1973, 36, 347-431.

123. Paszkowski, B. "Electron Optics"; Iliffe: London, 1968.

124. Pierce, J. R. "Theory and Design of Electron Beams"; van Nostrand: New York, 1949.

125. Read, F. H. J. Phys. E 1970, 3, 127-131; J. Phys. E 1971, 4, 562-566.

126. Saito, T.; Sovers, O. J. J. Appl. Phys. 1977, 48, 2306-2311.

127. Siegel, M. W., lecture notes, Extranuclear Laboratories, Inc., Pittsburgh, PA, November 1979; Pinnacle (Extranuclear Laboratories technical literature), October 1975, 2.

128. Spangenburg, K. R. "Vacuum Tubes"; McGraw-Hill: New York, 1948, Chapter 13.

129. Whitson, J. C.; Smith, J.; Whealton, J. H. J. Comp. Phys. 1978, 28, 408-415.

130. Alland, J. L.; Russell, R. D. Brit. J. Appl. Phys. 1963, 14, 800-804.

131. Paul, W.; Steinwedel, H. Z. Naturforsch. 1953, A8, 448-450.

132. Paul, W.; Reinhard, H. P.; von Zahn, U. Z. Phys. 1958, 152, 143-182.

133. Dawson, P. H., Ed. "Quadrupole Mass Spectrometry and Its Applications"; Elsevier: New York, 1976.

134. Dawson, P. H. Int J. Mass Spectrom. Ion Phys. 1971, 6, 33-44; Int. J. Mass Spectrom. Ion Phys. 1974, 14, 317-337; Int. J. Mass Spectrom. Ion Phys. 1975, 17, 423-445, 447-467; Int. J. Mass Spectrom. Ion Phys. 1976, 21, 317-332; J. Vac. Sci. Technol. 1972, 9, 487-491; J. Vac. Sci. Technol. 1974, 11, 1151-1153.

135. Majer, J. Talanta 1976, 23, 265-267.

136. Price, D.; Todd, J. F. J., Eds. "Dynamic Mass Spectrometry"; Heyden: London; Vols. 1-5, 1974-1978.

137. Kurz, E. A. Amer. Lab. March 1979, 11, 67-82.

138. Timothy, J. G.; Bybee, R. L. Rev. Sci. Instrum. 1978, 49, 1192-1196.

139. Gaydon, A. G. "Dissociation Energies and Spectra of Diatomic Molecules", 3'rd ed.; Chapman and Hall: London, 1968; Chapter 12.

140. Ahearn, A. J., Ed. "Trace Analysis by Mass Spectrometry"; Academic: New York, 1972.

ACKNOWLEDGEMENTS

The outstanding attribute of the Ames Laboratory is the spirit of willing cooperation that exists within and between research groups and support personnel. I owe thanks to many people for their assistance to my research, and I hope the following summary does them justice.

The patient encouragement of Drs. V. A. Fassel and H. J. Svec is gratefully acknowledged. I thank them for leaving me with an essentially independent command; however, they were always eager to assist me when asked. I also thank Chuck Taylor and the U. S. Environmental Protection Agency for their continued interest and generous financial support. The early stages of this research were littered with experimental problems, and I thank these people for bearing with me through this difficult period. I hope the eventual impact of this research justifies their trust.

At the tactical level, Alan Gray and Jerry Flesch contributed numerous suggestions and ideas. I thank them for unselfishly placing their extensive experience in mass spectrometry at my disposal. Tom Johnson constructed the various samples used in this research. He and Gary Wells contributed many suggestions for sampler design; these complemented their mechanical skill and perseverance in the sampler construction problems. Dave Birlingmaier and Kurt

Mogard designed and constructed the vacuum system. George Holland, Rick Ethington, and Fred Grabau helped with the installation and initial operation of the plasma. Greg Oestereich re-introduced me to computer programming and helped enormously in the writing and debugging of the program for reduction of the single ion data. I am most grateful for the cheerful and catalytic assistance of these people, without which my research would not have progressed very far. I also acknowledge the assistance of Mark Floyd and Betty Beymer in the preparation of this dissertation.

Finally, I thank my family for their interest and encouragement throughout my education. Special thanks are due to my father for his example of careful attention to detail, foresight, perfectionism, and indomitability. I hope my family shares the sense of pride and accomplishment that this research has generated in me.